Review Article: Computational Studies and DFT Calculations of Synthesized Triazolo Pyrimidine Derivatives: A Review

Hussein Shaban Mohamed[1,2]*, Zeinab Shaban Hamza[1], Amany Mohamed Nagdy[3], Hamada Rezk Abd El-Mageed[4]

[1]*Research Institute of Medicinal and Aromatic Plants (RIMAP), Beni-Suef University, Egyp*
[2]*Basic sciences department, Higher Technological Insitute-Beni Suef, Egypt*
[3]*Chemistry department, Faculty of science, Beni-Suef University, Egypt*
[4] *Micro-Analysis, Environmental Research and Community Afairs Center (MAESC), Faculty of Science, Beni-Suef University, Beni-Suef, Egypt*

Use yor device to scan and read the article online

Citation H.S. Mohamed*, Z.S. Hamza, A. Nagdy, H.R. Abd El-Mageed. **Computational Studies and DFT Calculations of Synthesized Triazolo Pyrimidine Derivatives: A Review.** *J. Chem. Rev.*, **2022**, *4*(2), 156-190.

https://doi.org/10.22034/JCR.2022.325439.1138

Article info:
Received: 19 January 2022
Accepted: 29 March 2022
Available Online: 20 April 2022
ID: JCR-2201-1138
Checked for Plagiarism: Yes
Language Editor:
Dr. Fatimah Ramezani
Peer Reviewers Approved by:
Dr. Parvin Hajiabbasi
Editor who Approved Publication:
Prof. Dr. Ghasem Rezanejade Bardajee

Keywords:
DFT, TD-DFT, Quantum mechanics calculations, Triazolo pyrimidine derivatives

ABSTRACT

In this study, we summarized the preparation, characterization, and computational research on triazolo pyrimidine derivatives utilizing the Density Functional Theory technique. Quantum mechanics calculations and thermodynamic parameters show that energy exchange takes place within molecules. Geometrical and structural aspects such as dipole moment, relative populations, relative total energies, electronic total energies, vertical emission energies, bond length, and bond angle were also discussed in this study. The triazolo pyrimidine ring is a structural characteristic found in a variety of active molecules with varying pharmacological activity. During the last few decades, a vast amount of published literature has been reviewed. This review covers numerous triazolo pyrimidine preparations, characterizations, and computational analyses, and it might be considered the lead compound for future medicinal and agrochemical development.

List of content

4. Conclusion

***Corresponding Author: Hussein Shaban Mohamed** (h_gendy_2010@yahoo.com)

1. Introduction

Triazolo pyrimidine derivatives are fused heterocyclic compounds which have found use in a range of industries [1-4]. Triazolo pyrimidines, 1,2,4-and 1,2,3-triazolopyrimidines, are utilized in anti-cancer [5-7] , anti-tumor [8], anti-inflammatory [9], anti-bacterial [10, 11], anti-fungal [12], and anti-malarial [13] therapeutic and pharmacological uses[6], [14-16]. They are anti-Leishmania [17, 18], anti-viral [19, 20], anti-HIV [21, 22] , anti-HCV [23], hypoglycemic [24-26] and have a microtubule-stabilizing CNS [26], [34]. Many biological applications make use of 1,2,4-triazolo [1,5-*a*] pyrimidine derivatives[27-32]. The spectroscopic properties of triazolo pyrimidine derivatives in the ultraviolet-visible (UV-vis) region were theoretically explored using Time-Dependent Density Functional Theory (TD-DFT) techniques to illustrate the influence of solvent polarity on UV-vis spectra [26]. The spectroscopic characteristics of triazolo pyrimidine metal complexes were also computed using the DFT and TD-DFT techniques [33, 34]. The electronic structure and UV–vis spectra of ruthenium(II) complexes bound to triazolo pyrimidine ligands were characterized using TD–DFT techniques [35, 36]. The anionic and neutral molecular orbital derivatives were constructed using molecular orbital theory at its B3LYP/6-311+G (d, p) level. Furthermore, the geometrical parameters obtained by DFT were compared to those obtained by X-ray structures [37, 38] and found to be in excellent agreement. The molecular orbitals of triazolo pyrimidine derivatives in the ground and excited states were also estimated at the B3LYP/6-31G level of theory [39, 40].

2. Experimental part for synthesis of triazolo pyrimidine

2.1. Synthesis of [1,2,3] triazolo[4,5-d] [1,2,4] triazolo[4,3-a] pyrimidine derivatives

3-benzyl-5-chloro-7-methyl-3*H*- [1,2,3] triazolo [4,5-*d*] pyrimidine may be produced by reacting benzylamine with boiling PrOH and then, diazotizing it in the presence of $NaNO_2$/HCl (**3**). Compound **3** was treated in boiling EtOH with hydrazine hydrate to provide the 2-hydrazino-substituted derivative (**4**) demonstrated in **Scheme 1** [41]. Chemical (**4**) reacts with CS_2 in dry pyridine to produce benzyl-9-methyl-3*H* [1,2,3] triazolo [4,5-*d*].triazolo [4,3-*a*]. 1-benzyl-4-methyl-1*H*-[1,2,3] triazolo [4,5-*e*] isomeric pyrimidine-7 (6*H*)-thione (**5**) 1-benzyl-4-methyl-1*H*-[1,2,3] triazolo [4,5-*e*] Pyrimidine-7 (6H)-thione, Triazolo [1,2,4] triazolo [4,3-a] pyrimidine-8 is demonstrated in **Scheme 2** [42].(7H)-thione (7).

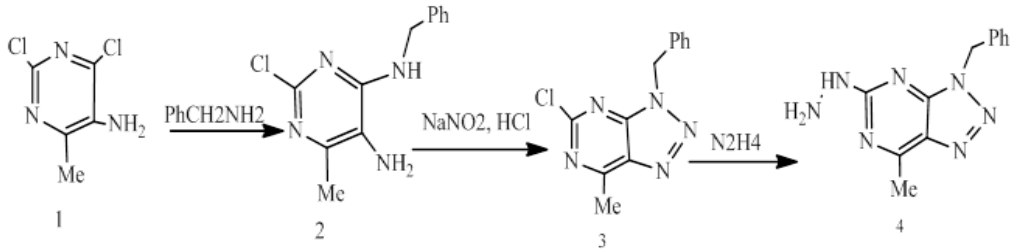

Scheme 1. Synthesis of 2-hydrazino-substituted derivative

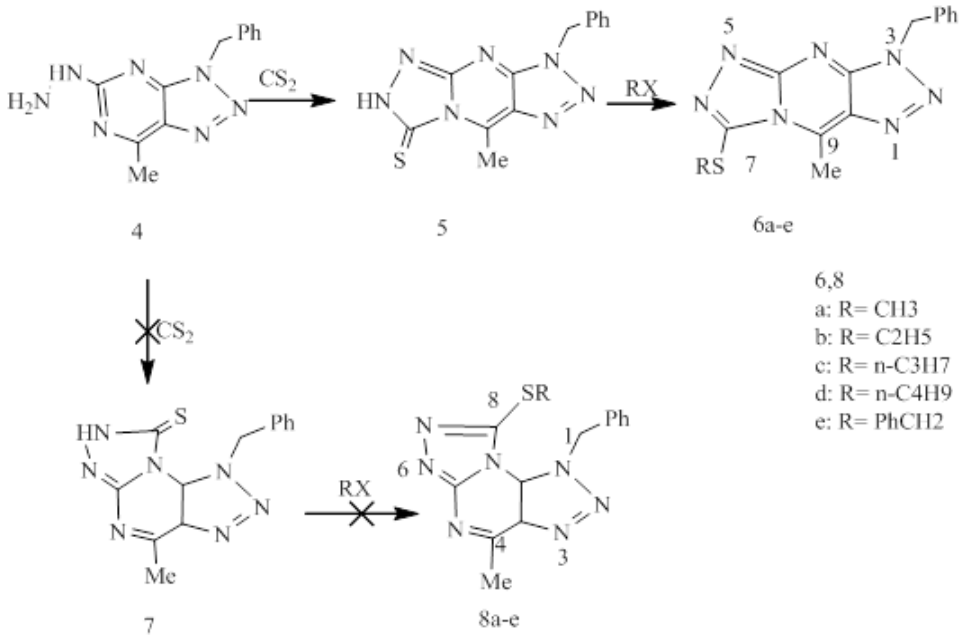

Scheme 2. Synthesis of benzyl-9-methyl-3*H* [1,2,3] triazolo [4,5-*d*] [1,2,4] triazolo[4,3-*a*] pyrimidine-7(6*H*)-thione

2.2. Synthesis of [1,2,4] triazolo [4,3-a] pyrimidine -5(1H) ones

In the presence of acetic acid, substituted 3,5-diamino [1,2,4] triazoles (**9**) react with beta keto esters, resulting in the addition of the keto ester to the more nucleophilic 3-amino group, followed by heterocyclization of enaminoester (10) to yield 2-substituted 3-amino [1,2,4] triazolo [4,3-*a*] pyrimidines (**11**) [41]. Triazolo pyrimidines undergo a more stable thermodynamic rearrangement to 1-substituted 3-amino-[1,2,4] tri-azolo [4,3-*a*] pyrimidines when heated (4) [42] Dimroth rearrangement can also occur, yielding 1-substituted 2-amino[1,2,4]triazolo[1,5-*a*]pyrimidines (**15**) [46]. This also happens when diamines (**9**) react with other 1,3-dicarbonyl compounds, as depicted in **Scheme 3** [43]. By reacting 3-alkylamino-5-amino-1-phenyl [1,2,4] triazoles (**6a**, **b**) with-keto esters (**15a-c**) and diethyl ethoxymethylenemalonate (**15d**), amino [1,2,4] triazolo pyrimidines with an alkyl substituent at the nitrogen atom of the pyrimidine or at the endocyclic amino group are produced. (Triazoles (**14a**, **b**) are heated with esters (**15a-d**) in the presence of acetic acid to produce 3-alkylamino-1-phenyl [1,2,4] triazolo[4,3-*a*] pyrimidin-5-ones, as shown in **Scheme 4** (**16a-f**). The yields of triazolo pyrimidines (**16a-f**) compounds are indicated in **Table 1**. Alkylamino triazoles (**14a**, **b**) react with dicarbonyl compounds, as shown in **Scheme 5** (**15a-d**). We may get triazolo pyrimidine from enaminoester (**17e**) by heating it at reflux in ethanol and then, heating it in the presence of acetic acid (**16e**). Condensation of triazoles (**14a**, **b**) with esters (**15a-d**) yielded triazolo pyrimidines (**16a-f**). The synthesis of enaminoesters (**17e**), which then cyclize to yield triazolo pyrimidines (**18**) as intermediates, appears to be the first step. Triazolo pyrimidines (**18**) recombine to generate more stable triazolo pyrimidines (**16**). 2-imino [1,2,4] triazolo [1,5-*a*] pyrimidines can be made by an unstable alternate chemical method (**19**) [44].

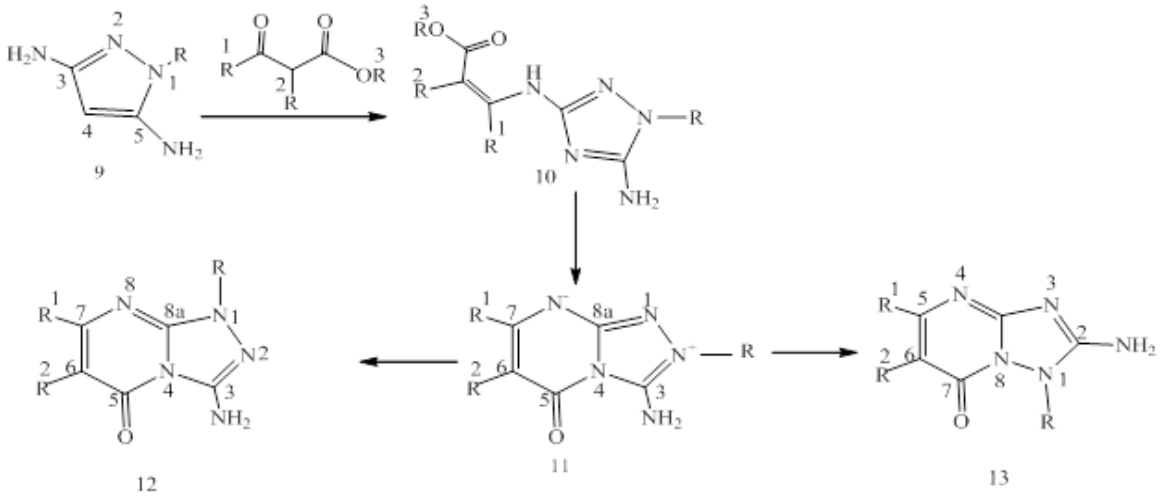

Scheme 3. Synthesis of 2-substituted 3-amino [1,2,4] triazolo[4,3-*a*] pyrimidines

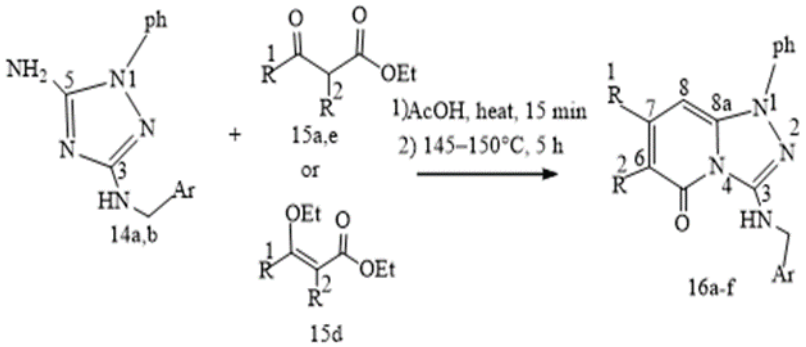

Scheme 4. Synthesis of 3-alkylamino-1-phenyl [1,2,4] triazolo[4,3-*a*] pyrimidin-5-ones

Table 1. Yields of triazolo pyrimidines **(16a-f)** compounds [45]

Starting compound		Product	Ar	R^1	R^2	Yield, %
Amine	Ether					
14a	**15a**	**16a**	Ph	Me	H	90
14b	**15a**	**16b**	4-ClC_6H_4	Me	H	78
14a	**15b**	**16c**	Ph	Pr	H	39
14a	**15c**	**16d**	Ph	CF_3	H	73
14a	**15d**	**16e**	Ph	H	CO_2Et	60
14b	**15d**	**16f**	4-ClC_6H_4	H	CO_2Et	49

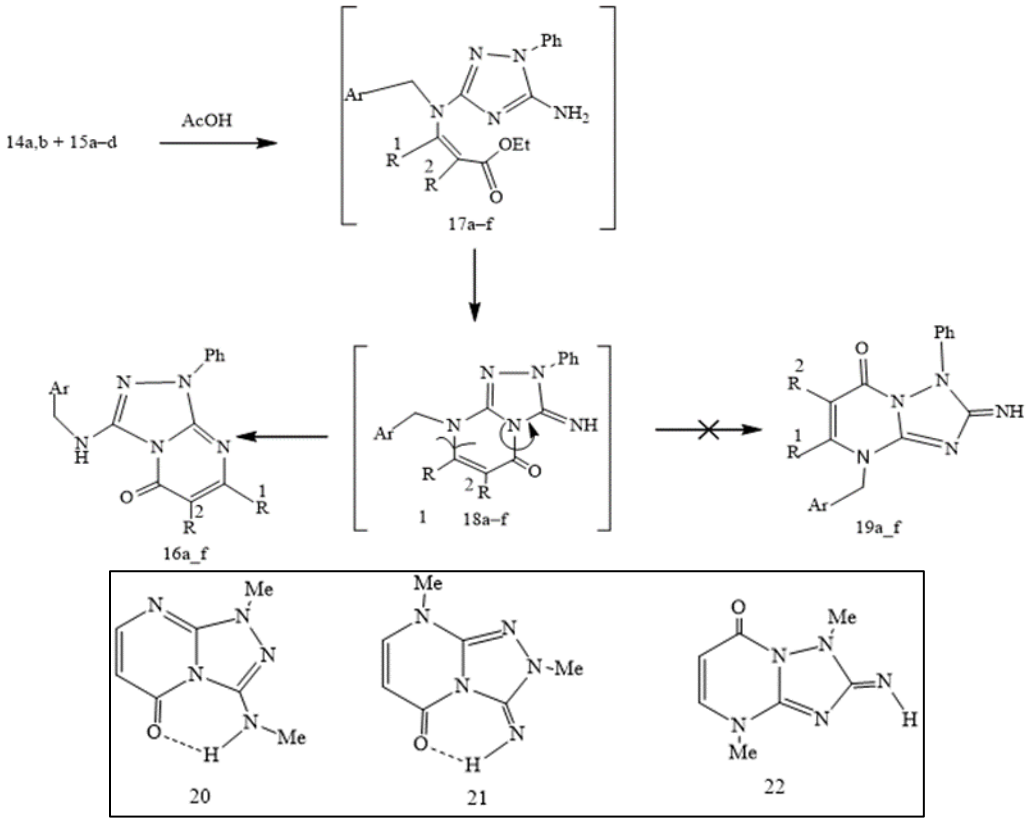

Scheme 5. Synthesis of triazolo pyrimidines **(16a-f)** and compounds **20-22**

2.3. Synthesis of [1,2,4]-triazolo[1,5-a] pyrimidines

The oxidative cyclization of appropriate *N*-benzylidene-*N*-pyrimidin-2-yl hydrazine precursors was followed by the preparation of novel [1,2,4]-triazolo-[1,5-*a*] pyrimidine derivatives. As demonstrated in **Scheme 6** [45], a Dimroth adjustment occurs.

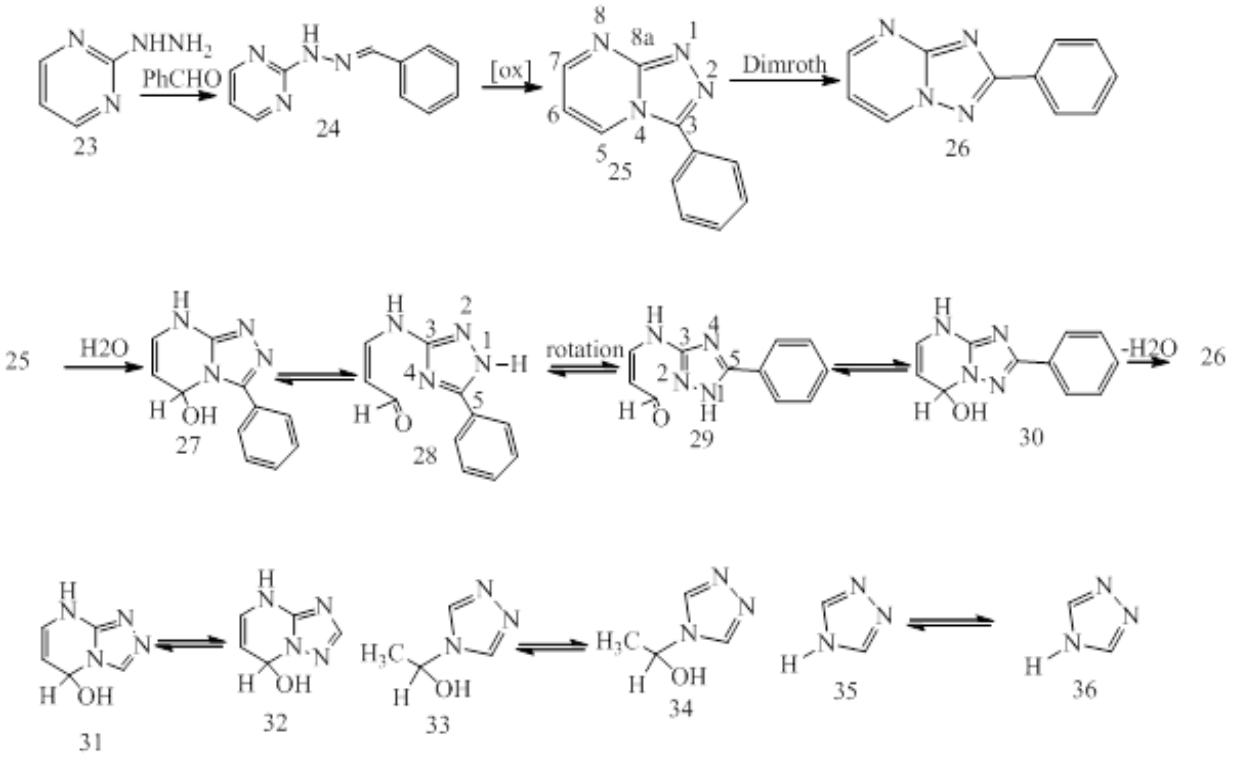

Scheme 6. Synthesis of [1,2,4]-triazolo-[1,5-*a*] pyrimidine derivatives

We made hydrazine (**38**) from 2-chloro-5-bromopyrimidine (**37**) and condensed it with substituted benzaldehydes to get hydrazones (**39**). Hydrazones (**39a–d**) were cyclized to [1,2,4]-triazolo[4,3-*a*] pyrimidines (**40a–d**) using [1.1]. By reacting the 6-bromo[1,2,4]-triazolo[1,5-*a*] pyrimidines (**40a–c**) with alkyl amines, compounds (**41a–c**) were formed. The hydroxyl derivative was obtained by demethylating compound (**41a**) with BBr_3 (**41d**). As indicated in **Scheme 7**, MW irradiation of the bromo derivative (**40d**) with an aliphatic amine produced the 7-amino derivatives (**43e–g**). The van der Plas' ANRORC process [46-48] occurred when the substitution occurred in the t position of the leaving group.

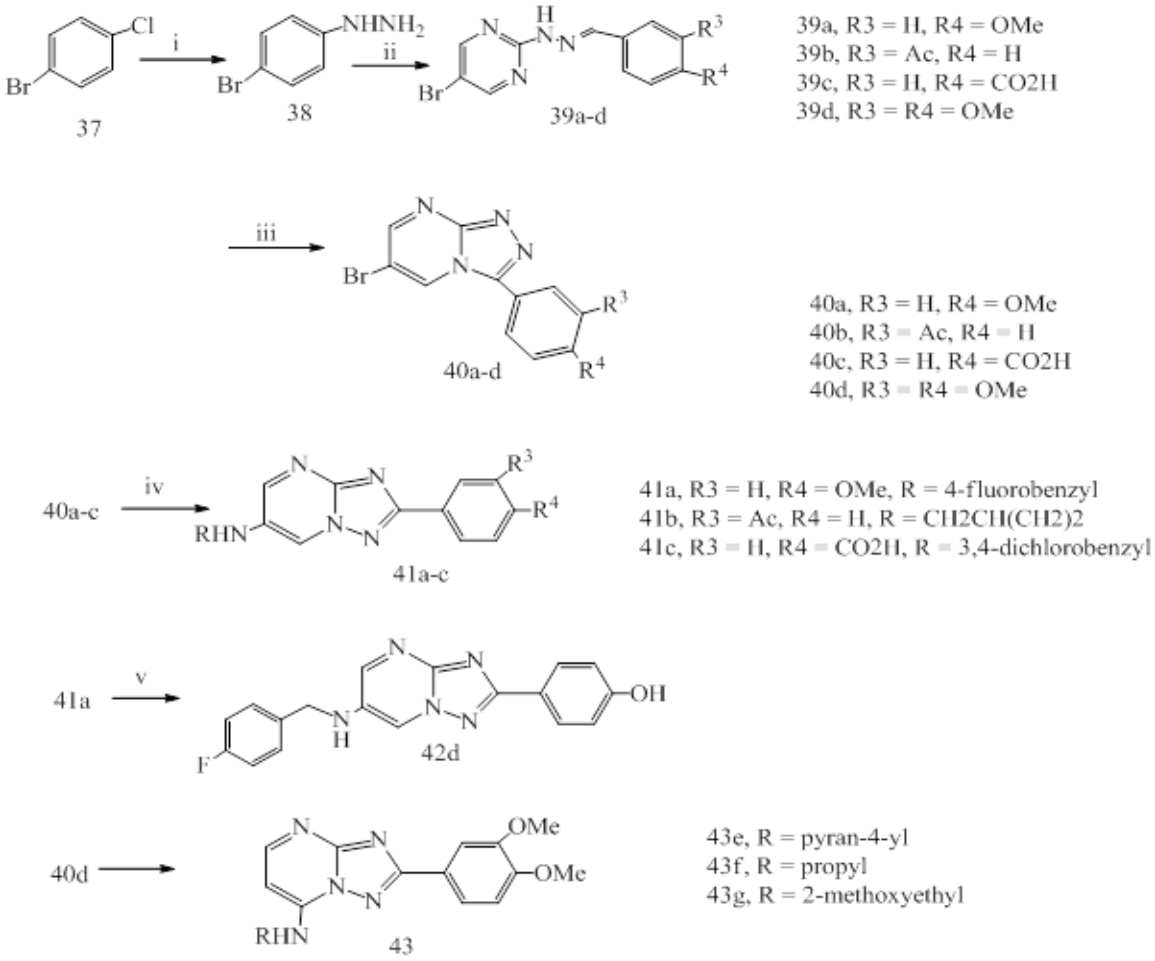

Scheme 7. Synthesis of **(43e–g)** derivatives

2.4. Synthesis of [Re (CO)$_3$L$_2$Cl] (L = 1,2,4-triazolo-[1,5-a] pyrimidine)

(0.2 g, 0.55 mmol) of Re(CO)$_5$Cl and (0.114 g, 1.16 mmol) of 1,2,4-triazolo-[1,5-*a*] pyrimidine were refluxed for 6 hours in toluene (80 ml) [49].

2.5. [1,2,4]-Triazolo[1,5-a] pyrimidine derivatives

Inhibition of mild steel corrosion was carried out by 1,2,4-triazolo[1,5-*a*]pyrimidine derivatives (P3 and P4) in 1 M HCl solution [50].

2.6. Synthesis of [1,2,4] triazolo-[1,5-a] pyrimidine and 5,7-dimethyl- [1,2,4] triazolo- [1,5-a] pyrimidine

[1,2,4]triazolo-[1,5,*a*]pyrimidine (tp) and 5,7-dimethyl-[1,2,4]triazolo-[1,5,*a*]pyrimidine (dmtp) react with diorganotin dichloride to form Me$_2$SnCl$_2$(tp)$_2$, Et$_2$ SnCl$_2$(tp)$_2$, Me$_2$ SnCl$_2$(dmtp)$_2$, Et$_2$ SnCl$_2$(dmtp)$_2$, Bu$_2$SnCl$_2$(dmtp), Ph$_2$SnCl$_2$(dmtp) [51].

2.7. Synthesis of triazolo[1,5-a] pyrimidine derivatives

The seven compounds were made using methods described in the literature [52]. Two fused triazolo pyrimidine rings are connected to two terminal phenyl groups through a pyrimidine ring in the suggested molecules. The effect of substitutes is explored. The structure of the seven suggested triazolo [1,5-*a*] pyrimidine

derivatives (**45–51**) is revealed by the insertion of different substituents attached beside position 4 to both phenyl groups, Ph-X and Ph-Y, in which molecule. As demonstrated in **Scheme 8.** (**45**) is 5,7-diphenyl-4,7-dihydrofuran-[1,2,4]. 5-(4-fluorophenyl)-7-(4-nitrophenyl)-4,7-dihydro-[1,2,4] pyrimidine (**46**) is 5-(4-fluorophenyl)-7-(4-nitrophenyl)-4,7-dihydro-[1,2,4] pyrimidine (**46**) is 5-(4-fluorophenyl)-7-(4-nitrophenyl)(**47**) is 5-(4-fluorophenyl)-7-(4-methoxyphenyl)-4,7-dihydro-[1,2,4] triazolo [**1,5-*a***] pyrimidine, (**48**) is 5,7-bis(4-fluorophenyl)-4,7-dihydro-[1,2,4] triazolo [**1,5-*a***] pyrimidine, and (**49**) is 7-(4-brom(**50**) is 5-(4-fluorophenyl)-7-(*p-tolyl*)-4,7-dihydro-[1,2,4] pyrimidine triazolo.

Triazolo pyrimidine compounds	X	Y
45	H	H
46	NO_2	F
47	OCH_3	F
48	F	F
49	Br	F
50	CH_3	F
51	F	OCH_3

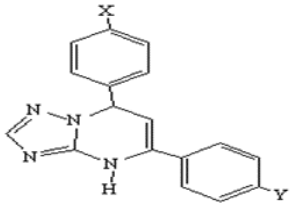

44

Scheme 8. Synthesis of triazolo[1,5-*a*] pyrimidine derivatives which, under investigation in this part

2.8. Synthesis of amino [1,2,4] triazolo[1,5-a] pyrimidines

To get mesoionic compounds (**57a-e**) as well as (**56c-f**), cations of compounds (**55a-e**) and (**56c-f**) were deprotonated at the amide nitrogen in aqueous sodium carbonate solutions at ambient temperature (**58c-f**). As demonstrated in **Scheme 9**[53] , cations of compounds (**59a,g,h**) lost a proton from the NH group of the dihydropyrimidine moiety to provide free bases (**60 a,g,h**).

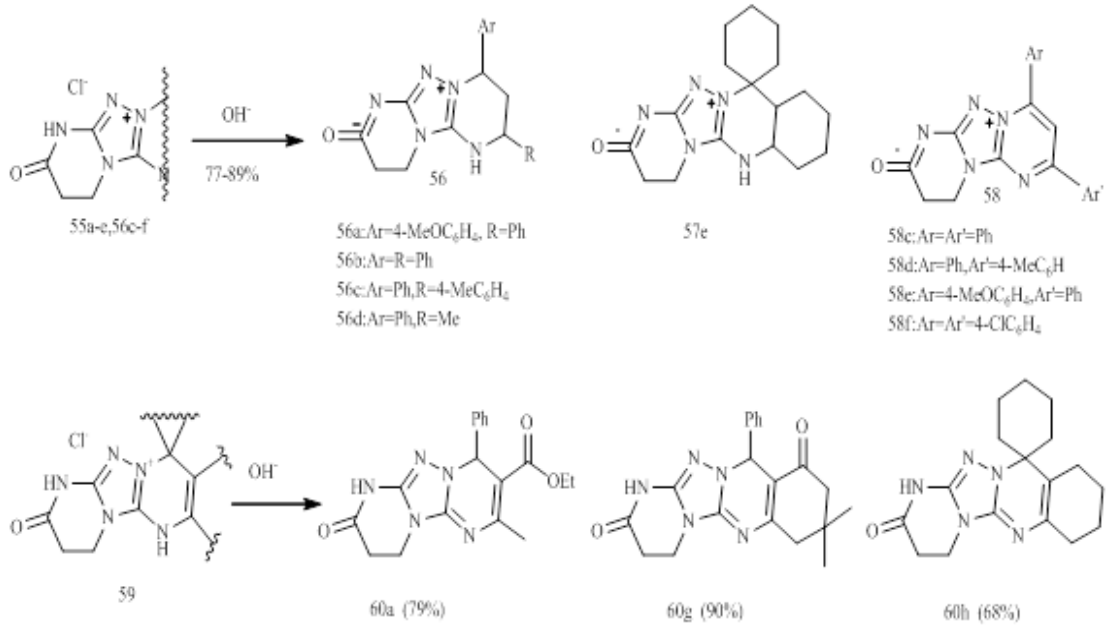

Scheme 9. Synthesis of free bases of (**60a, g, h**) compounds

2.9. Synthesis of amino [1,2,4] triazolo[1,5-a] pyrimidines

By reacting 2-aminosubstituted [1,2,4] triazolo[1,5-*a*] pyrimidines (**61**) with their counterparts in acid medium with varying pyrimidine ring saturation and 1,3-diketones or 1,1,3,3-tetramethoxypropane, variably substituted polycyclic derivatives of triazolo pyrimidine were synthesized. As demonstrated in **Scheme 10**. The reaction of 4,5,6,7-tetrahydro- or aromatic amino triazolo pyrimidines with a cascade rearrangement with recyclization of the dihydropyrimidine ring yields partially hydrogenated [1,2,4]triazolo[1,5-*a*:4,3-*a*']dipyrimidin-5-ium salts, and the reaction of substrates containing the4,7-dihydro-[1,2,4]triazolo. As demonstrated in **Scheme 11**[54].

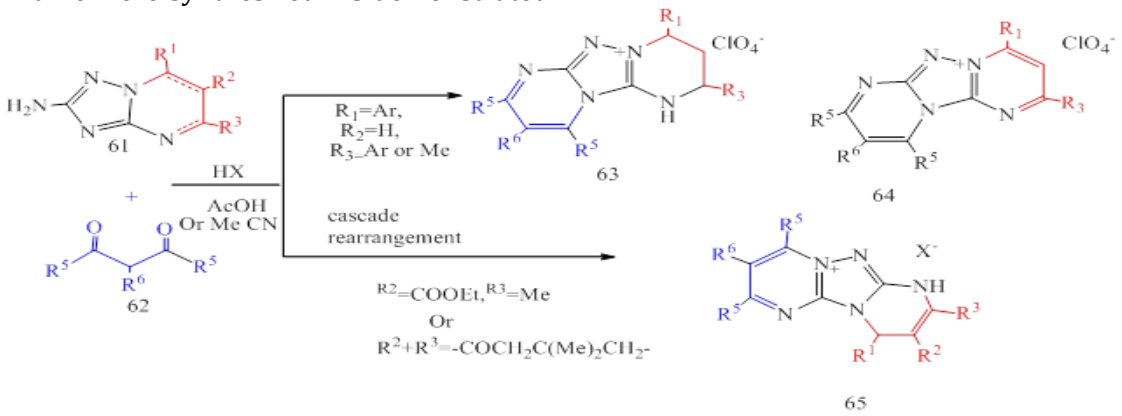

Scheme 10. Synthesis of [1,2,4] triazolo[1,5-*a*:4,3-*a*`] dipyrimidin-5-ium or 1,2,4] triazolo[3,4-*b*] quinazolin-5-ium salts

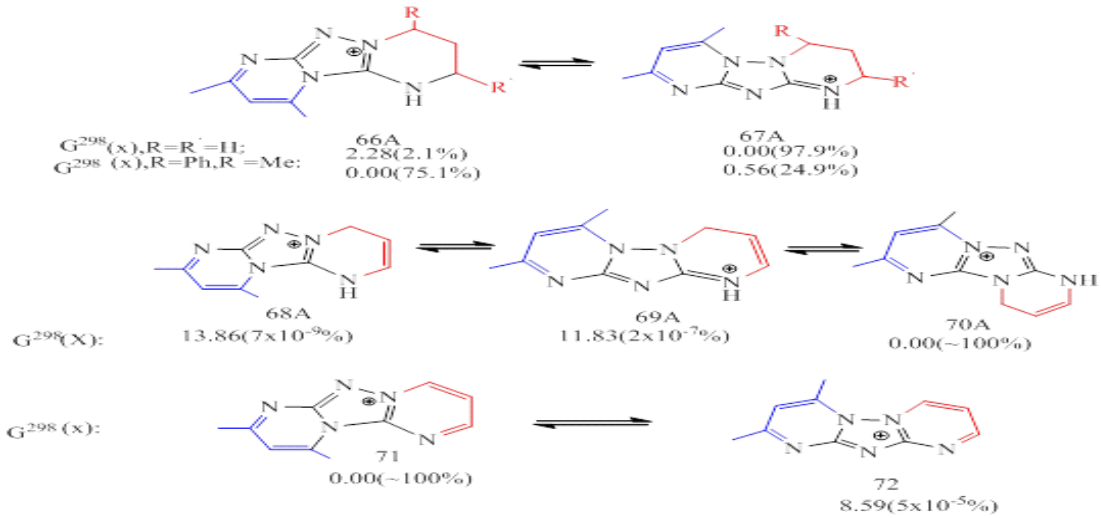

Scheme 11. [1,2,4] triazolo[1,5-*a*:4,3-*a*`] dipyrimidin-5-ium or 1,2,4] triazolo[3,4-*b*] quinazolin-5-ium salts yield

2.10. Amino [1,2,4] triazolo[1,5-a]-pyrimidines

2-Amino-substituted triazolo pyrimidines **(73–75)** with various saturation of the pyrimidine fragment (**Scheme 12**) is used for the synthesis of substituted triazolo pyrimidines [1-3] and their polycyclic derivatives [**4-7**]. Compounds **(73–75)** were obtained by reactions of 3,5-diamino-1,2,4-triazole with many saturation of the pyrimidine ring was obtained by oxidation or hydrogenation of the dihydro derivatives as shown in **Scheme 12** [55-57].

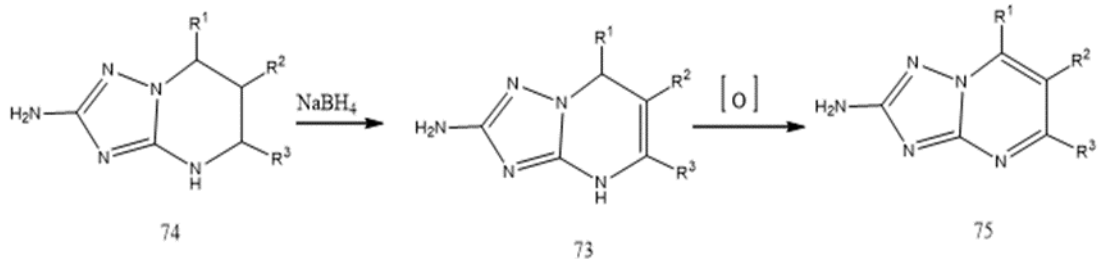

Scheme 12. Synthesis of 2-amino-substituted triazolo pyrimidines

2.11. Synthesis of R-7-methyl [1,2,4] triazolo[2,3-a] pyrimidines

5-R-3-amino-1,2,4-triazoles (**76**) regioselectively reacted with ethoxymethylidene acetylacetone and ethyl ethoxymethylidene acetoacetate to provide 2-*R*-7-methyl [1,2,4] triazolo[2,3-*a*] pyrimidines, as indicated in **Scheme 13**. Reflux of compounds (**76a-f**) with ethoxy methylidene acetylacetone or ethyl ethoxymethylidene acetoacetate in acetic acid for 40-60 minutes provides the corresponding 2-*R*-7-me-thyl[1,2,4]triazolo[2,3-*a*]pyrimidines (**84**) in high yields, regardless of the substituent R, as indicated in **Scheme 14** [58].

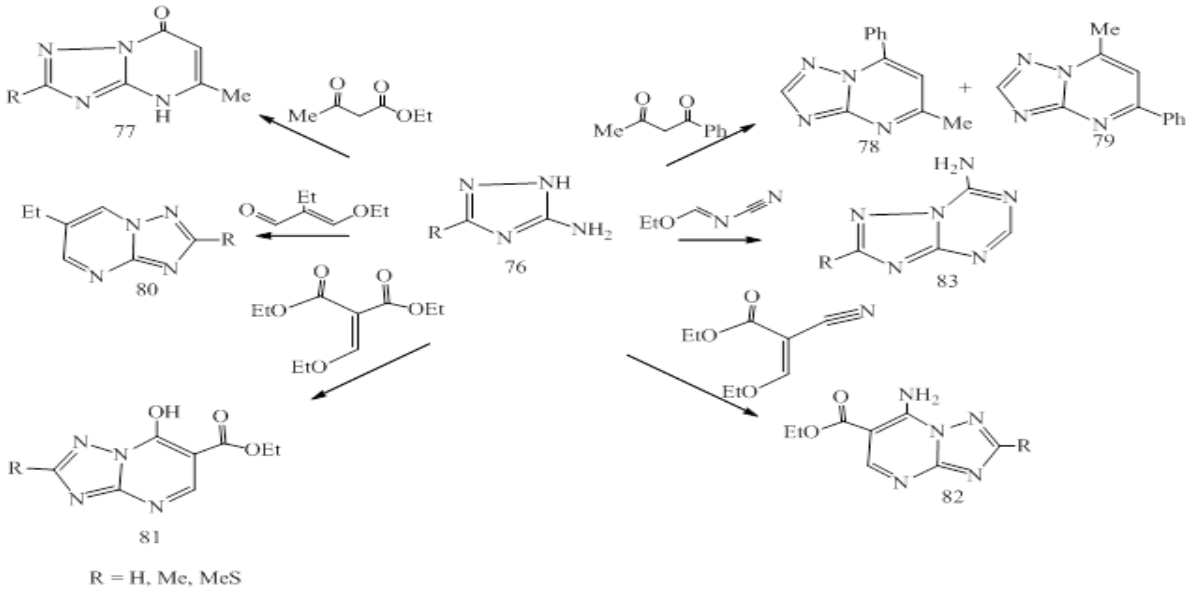

Scheme 13. Synthesis of 2-R-7-methyl [1,2,4] triazolo[2,3-*a*] pyrimidines

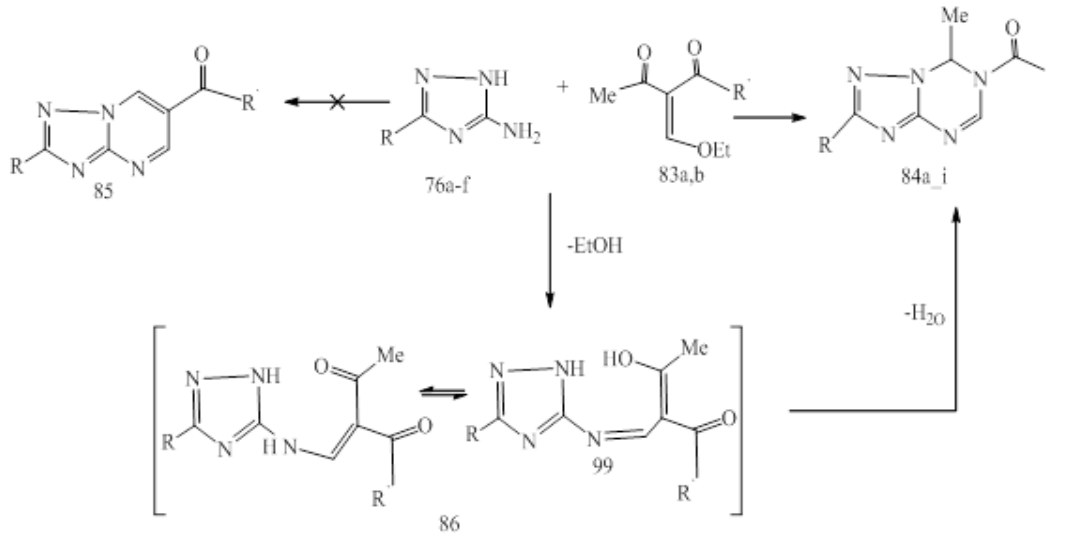

76: R = H (a), Me (b), CF3 (c), MeS (d), PhCH2S (e), EtS (f); 84: R = H, R´ = Me (a), R = R´ = Me (b), R = CF3, R´ = Me (c), R = H, R´ = OEt (d), R = Me, R´ = OEt (e), R = CF3, R´ = OEt (f), R = MeS, R´ = Me (g), R = PhCH2S, R´ = Me (h), R = EtS, R´ = OEt (i); 83: R´ = Me (a), OEt (b)

Scheme 14. Yield of 2-*R*-7-methyl [1,2,4] triazolo[2,3-*a*] pyrimidines and 2-*R*-7-methyl [1,2,4] triazolo[2,3-*a*] pyrimidines

2.12. Synthesis of thieno[3,2-e] [1,2,4] triazolo[1,5-c] pyrimidines

Both nucleophilic and electrophilic agents can trigger the recyclizations, which follow the same steps: nucleophile (electrophile) ring opening ring closure (paths A and B) as indicated in **Scheme 15** [59, 60].

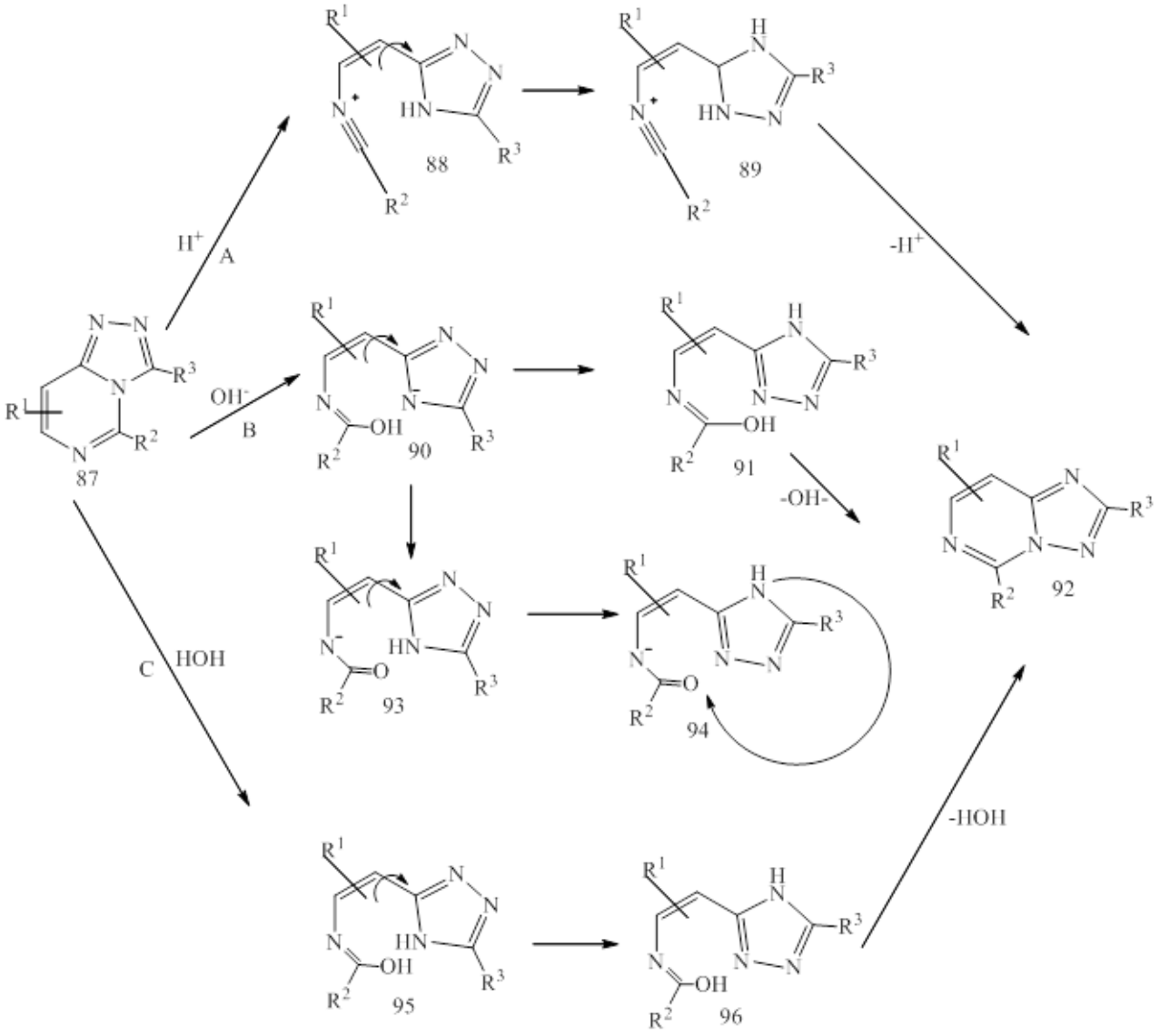

Scheme 15. The recyclizations paths of the addition of nucleophile (electrophile) ring opening ring closure (paths A and B)

2.2. Computational evaluations

*2.2.1. (**6a–e**) and (**8a–e**) compounds*

DFT calculations in the solvent phase were performed using the Polarizable Continuum Model (PCM) at the B3LYP-6-311+g (2d, p) level of theory to compute the proton chemical shifts of (**6a–e**) and (**8a–e**) compounds. The resulting results agreed well with the experimental data. (**6a–e**) compounds are more thermodynamically favorable than (8a–e) compounds based on the relative Gibbs free energy [61, 62]. **Table 2** indicates the chemical shifts of the two benzylic hydrogens on the carbon linked to nitrogen N-3 in (**8a–e**) or nitrogen N-1 in (**8a–e**). Cyclisation reaction occurs in such a way that the anthracene-like hetero-cycle is formed.

Table 2. Experimental and theoretical ^{1}HNMR chemical shifts in ppm relative to TMS for benzylic protons (on carbon attached to nitrogen N-3 of (**8a-e**) or nitrogen N-4 of (**6a-e**) in PCM (chloroform)/ B3LYP/6-311+g (2d, p)

Compound	Experimental		Theoretical	
	Benzylic	Integration	chemical shifts [a]	chemical shifts [b]
6a	5.83	2	5.86	5.84
8a			6.15	6.39
6b	5.83	2	5.85	5.83
8b			6.14	6.50
6c	5.83	2	5.85	5.83
8c			6.27	6.71
6d	5.83	2.02	5.88	5.84
8d			6.27	6.70
6e	5.84	2	5.66	5.60
8e			6.34	6.44

[a] Adjacent proton to nitrogen N-4 of **6a–e**.
[b] Adjacent proton to sulfur atom in (**8a–e**).

*2.2.2. Compounds (**20-22**)*

To determine the thermodynamic likelihood of production of isomers (**8**), (**10**), and (**12**), quantum-chemical calculations for the energy parameters of model compounds (**20**), (**21**) and (**22**) were performed (**11**). **Table 3** displays the computed relative Gibbs energies (G298), dipole moments, and relative concentrations (x) of hypothetical equilibrium mixes of isomers (**20**, **21**, and **22**) in gas and aqueous phases. It was discovered that isomer (**20**) is more stable in nonpolar solvents and aqueous solutions than isomers (**21**) and (**22**) and that its equilibrium concentration approaches 100%. Isomer (**21**) is thermodynamically more stable (3.9-5.0 kcal/mol) than isomer (**22**) due to intra-molecular hydrogen bonding. The difference in free energy between isomeric amino triazolo pyrimidines 3-5 (3.6-4.9 kcal/mol) and alkyl amino triazolo pyrimidine (**20**) and imino isomers (**21**) (9.8 kcal/mol) and (**22**) (13.6 kcal/mol) is greater than the difference in free energy between isomeric amino triazolo pyrimidines 3-5 (3.6-4.9 kcal/mol) [63].

Structures of model molecules **(20), (21)**, and **(22)** (intra-molecular hydrogen bonds are indicated in the **Scheme 5**).

Table 3. Relative Gibbs Energies ΔG^{298}, Dipole Moments μ and Relative Concentrations x in Equilibrium Mixtures of Isomers (**20**), (**21**) and (**22**) at 298K

Isomer	ΔG^{298} kcal/mol	μ D	x %	Isomer	ΔG^{298} kcal/mol	μ D μ, D	x %
Gas phase				water phase			
20	0.00	2.52	~100	20	0.00	3.36	~100
21	13.50	7.14	1.3×10^{-8}	21	9.77	10.41	6.7×10^{-6}
22	18.51	6.76	2.7×10^{-12}	22	13.62	9.78	1.0×10^{-8}

2.2.3. [1,2,4] Triazolo[1,5-c] pyrimidine

[1,2,4]-triazolo[4,3-*c*] pyrimidine rearrangement to [1,2,4]-triazolo[4,3-*c*] pyrimidine rearrangement. The hypothesis of triazolo[1,5-c]pyrimidine was investigated at the B3LYP/6-31G(d,p) level [64]. Diverse processes (neutral, acidic, and basic), as well as solvent effects, all point to an ANRORC mechanism for the Dimroth rearrangement. The right-side isomers are more stable than the left side isomers in the three equilibriums of (**Scheme 8**): XI contains 48.4 kJ mol^{-1}, XIII has 50.1 kJ mol^{-1}, and XV contains 28 kJ mol^{-1}. As depicted in **Table 4, 43a–g** the [1,5-*a*], isomer is more stable than [4,3-*a*] between 60 and 62 kJ

mol^{-1}. **Table 5** reveals that the [1,5-*a*] isomers are more stable than the [4,3-*a*] isotopes between 57 and 69 kJ mol^{-1} [65] for 6-bromo derivatives (**40a–d**).

Table 4. Total energy (Hartree) and relative energy (kJ mol^{-1}) of the [1,2,4] triazolo[1,5*a*] pyrimidine, (**43a–g**), and the (hypothetical) [1,2,4]-triazolo [4,3] pyrimidine isomers (**43a–g** bis)

	E_{total}		E_{total}	E_{rel}
43a	—1182.7673	5a	—1182.7441	61.01
43b	—1007.2537	5b	—1007.2301	62.24
43c	—2076.8182	5c	—2076.7946	62.54
43d	—1143.4584	5d	—1143.4348	61.45
43e	—1198.2557	5b	—1198.2325	61.00
43f	—1045.5864	5c	—1045.5631	61.12
43g	—1120.8094	5d	—1120.80942	60.42

Table 5. Total energy (hartree) and relative energy (kJ mol^{-1}) of the [1,2,4]-triazolo [4,3- *a*] pyrimidine, (**40a–d**), and their [1,2,4]-triazolo[1,5-*a*] pyrimidine counterparts, (**40a–d** bis) [70]

	E_{total}		E_{total}	E_{rel}
40a	—3331.21619	4a bis	—3331.24031	63.34
40b	—3405.29446	4b bis	—3405.31894	64.29
40c	—3369.34943	4c bis	—3369.37137	57.60
40d	—3445.76584	4d bis	—3445.79199	68.65

2.2.4. [1,2,4]-triazolo [1,42 a] pyrimidine isomer

Table 6 indicates theoretical statistics for the hypothetical [4,3-*a*] isomer of (**42a**) (**42a** bis). We find that the estimated ^{13}C and ^{15}N chemical shifts for the [1,2,4]-triazolo [1,42 *a*] pyrimidine isomer geometry match those found experimentally, however the states of (**5b and 5c** bis) differ significantly, as reported in **Tables 7, 8, 9 and 10** [66, 67].

Table 6. Measured chemical shifts of compound (**5a**), and absolute shielding and calculated chemical shifts for the [1,5-*a*] and the (hypothetical) [4,3-*a*] structures

Predict for [1,2,4]-triazolo [1,5-*a*] pyrimidine scaffold				Predict for [1,2,4]-triazolo [4,3-*a*] pyrimidine scaffold				
Atom number	Atom position	Calc. shielding	б(calc.)	Atom number	Atom position	Calc. shielding	б(calc.)	б(exp)
1	N-1	0.73	—125.7	1	N-1	—100.95	—56.2	—153
2	C-2	10.9	165.2	2	N-2	—127.25	—31.2	163.4
3	N-3	—37.9	—116.0	3	C-3	33.02	143.9	—115.8
4	N-4	2.58	—154.4	4	N-4	59.39	208.4	n.d.
5	C-5	66.25	111.9	5	C-5	75.13	103.3	114.2
6	C-6	43.78	133.5	6	C-6	43.99	133.3	135.5
7	C-7	33.9	143.1	7	C-7	34.42	142.6	148.2
8	N-8	-58.96	-96.0	8	N-8	- 68.21	-87.3	-104
9	C-8a	24.4	152.2	9	C-8a	24.99	151.6	150.5
10	H-7	23.63	8.1	10	H-7	23.71	8.0	8.57
11	H-5	23.94	7.8	11	H-5	24.21	7.6	8.36
12	Ph C-1	52.63	125.0	12	Ph C-1	55.79	122.0	123.8
13	Ph C-2	50.14	127.4	13	Ph C-2	45.06	132.3	128.1
14	Ph C-6	47.23	130.2	14	Ph C-6	53.39	124.3	128.1
15	Ph H-6	23.08	8.6	15	Ph H-6	23.62	8.1	8.05
16	Ph H-4	23.36	8.3	16	Ph H-4	24.26	7.5	8.05
17	Ph C-5	71.53	106.8	17	Ph C-5	58.43	119.4	114.5
18	Ph C-3	61.05	116.9	18	Ph C-3	72.36	106.0	114.5
19	Ph H-5	25.22	6.5	19	Ph H-5	24.54	7.2	7.06

20	Ph H-3	24.83	6.9	20	Ph H-3	25.18	6.6	7.06
21	Ph C-4	14.07	162.2	21	Ph C-4	15.28	161.0	160.9
22	OCH_3	126.89	53.5	23	OCH_3	127.21	53.2	55.7
23	OCH_3	28.22	3.6	24	OCH_3	28.23	3.6	3.82
24	OCH_3	28.22	3.6	25	OCH_3	28.25	3.6	3.82
25	OCH_3	27.83	4.0	26	OCH_3	27.78	4.1	3.82
26	C-6-NH	172.3	-315.5	27	C-6-NH	170.28	-313.6	-281.4
27	C-6-NH	28.99	2.9	28	C-6-NH	28.93	2.9	112.3
28	$NHCH_2$	131.37	49.2	29	$NHCH_2$	131.42	49.1	46.2
29	$NHCH_2$	27.66	4.2	30	$NHCH_2$	27.69	4.1	4.31
30	$NHCH_2$	28.18	3.7	31	$NHCH_2$	28.36	3.5	4.31
31	Bn C-1	43.28	134.0	32	Bn C-1	43.8	133.5	134.9
32	Bn C-2	46.15	131.3	33	Bn C-2	46.25	131.2	129.6
33	Bn C-6	46.82	130.6	34	Bn C-6	47.26	130.2	129.6
34	Bn H-2	24.14	7.6	35	Bn H-2	24.09	7.6	7.49
35	Bn H-6	24.44	7.3	36	Bn H-6	24.47	7.3	7.49
36	Bn C-5	62.68	115.3	38	Bn C-5	62.76	115.3	115.2
37	Bn H-3	24.63	7.1	39	Bn H-3	24.68	7.1	7.19
38	Bn H-5	24.72	7.0	40	Bn H-5	24.81	6.9	7.19
39	Bn C-4	10.66	165.4	41	Bn C-4	10.06	166.0	161.5

Table 7. Absolute shielding, calculated and measured chemical shifts of compound (**5b** and **5c**)

Atom number	Atom position	Calc. shielding	б(calc.)	б(exp.)	Atom number	Atom position	Calc. shielding	б(cal.)	б(exp.)
1	N-1	—0.82	—151.2	n.d.	1	N-1	—5.55	—146.7	n.d.
2	C-2	12.31	163.8	162	2	C-2	11.69	164.4	162
3	N-3	— 40.64	—113.4	—112.6	3	N-3	—43.8	—110.4	n.d.
4	N-4	1.71	—153.6	—152.1	4	N-4	2.05	_153.9	_151.9
5	C-5	67.63	110.6	113.9	5	C-5	66.04	112.1	114.3
6	C-6	43.25	134.1	137	6	C-6	43.18	134.1	136.2
7	C-7	34.11	142.9	149.4	7	C-7	32.78	144.1	148.5
8	N-8	—60.17	—94.9	—102.7	8	N-8	—62.34	—92.8	—101.8
9	C-8a	25.17	151.5	151.3	9	C-8a	24.74	151.9	151.3
10	H-7	23.6	8.1	8.6	10	H-7	23.52	8.2	8.64
11	H-5	24.11	7.6	8.43	11	H-5	23.96	7.8	8.42
12	PhC-1	44.88	132.5	132	12	Ph C-1	40.07	137.1	135.2
13	Ph H-6	47.24	130.2	130.9	13	Ph C-2	52.29	125.3	126.7
14	Ph C-4	47.83	129.6	126	14	Ph C-6	49.69	127.8	126.7
15	Ph H-6	23.15	8.5	8.36	15	Ph H-2	23.21	8.5	8.23
16	Ph H-2	22.55	9.1	8.67	16	Ph H-6	23.03	8.7	8.23
17	Ph C-5	50.52	127.0	129.6	17	Ph C-3	46.2	131.2	130.2
18	Ph H-5	24.28	7.4	7.68	18	Ph C-5	46.66	130.8	130.2
19	PhC-4	48.06	129.4	129.7	19	Ph H-3	23.41	8.3	8.06
20	Ph<u>H</u>-4	23.26	8.4	8.06	20	Ph H-5	23.53	8.2	8.06
21	PhC-3	41.03	136.2	137.6	21	Ph C-4	48.93	128.6	132.4
22	$COCH_3$	—19.39	194.4	198.2	22	COOH	12.08	164.1	167.6
23	C<u>O</u>CH_3	— 298.4			23	C<u>O</u>OH	—72.75		
24	$COCH_3$	155.34		27.3	24	CO<u>O</u>H	126.22		
25	COC<u>H</u>$_3$	29.03	2.8	2.66	25	COO<u>H</u>	26.24	5.5	13.1
26	COC<u>H</u>$_3$	29.03	2.8	2.66	26	C-6-<u>N</u>H	173.17	—316.3	_321.4
27	COC<u>H</u>$_3$	29.69	2.2	2.66	27	C-6-N<u>H</u>	28.9	3.0	6.99
28	C-6-<u>N</u>H	179.58	—322.4	—318.6	28	$NHCH_2$	131.87	48.7	45.7
29	C-6-N<u>H</u>	28.69	3.2		29	NHC<u>H</u>$_2$	27.7	4.1	4.37
30	NH–CH_2	130.96	49.6	48.2	30	NHC<u>H</u>$_2$	28.29	3.6	4.37

31	NH-CH$_2$	29.84	2.1	2.92	31	Bn C-1	40.26	136.9	140.1
32	NH–CH$_2$	28.45	3.4	2.92	32	Bn C-2	46.31	131.1	129.9
33	CH	169.22	12.7	10.2	33	Bn C-6	50.63	126.9	128.4
34	CH	31.01	0.9	1.12	34	Bn H-2	24.09	7.6	7.73
35	(CH$_2$)$_2$	176.84	5.4	3.9	35	Bn C-3	24.7	7.0	7.44
36	(CH$_2$)$_2$	31.01	0.9	0.53	36	Bn C-3	34.21	142.8	130.1
37	(CH$_2$)$_2$	31.55	0.4	0.27	37	Bn C-5	47.07	130.4	131
38	(CH$_2$)$_2$	178.1	4.2	3.9	38	Bn H-5	24.43	7.3	7.64
39	(CH$_2$)$_2$	31.33	0.6	0.53	39	Bn C-4	34.84	142.1	131.2
40	(CH$_2$)$_2$	31.64	0.3	0.27	40	Bn 4-Cl	678.58		

Table 8. The experimental and optimized bond lengths [Å] and angles [°] for [Re (CO)$_3$(tp)$_2$Cl]

Experimental		Optimized		Experimental		Optimized	
Bond lengths		B1	B2	Bond angles		B1	B2
Re (1)–C (1)	1.924	1.921	1.925	C (2)–Re (1)–C (1)	90.13	90.74	89.87
Re (1)–C (2)	1.893	1.915	1.918	C (2)–Re (1)–C (3)	88.49	90.30	89.47
Re (1)–C (3)	1.913	1.918	1.924	C (3)–Re (1)–C (1)	91.05	90.22	89.65
Re (1)–Cl (1)	2.490	2.546	2.544	C (1)–Re (1)–N (1)	91.20	92.25	93.16
Re (1)–N (1)	2.191	2.248	2.239	C (2)–Re (1)–N (1)	91.75	93.86	93.93
Re (1)–N (5)	2.197	2.256	2.248	C (3)–Re (1)–N (1)	177.74	175.13	175.60
C (1)–O (1)	1.157	1.161	1.166	N (1)–Re (1)–N (5)	84.08	85.31	84.31
C (2)–O (2)	1.158	1.166	1.168	N (1)–Re (1)–Cl (1)	86.15	84.18	84.71
C (3)–O (3)	1.159	1.162	1.167	C (1)–Re (1)–Cl (1)	92.28	92.98	92.54
				C (2)–Re (1)–Cl (1)	176.84	175.86	177.29
				C (3)–Re (1)–Cl (1)	93.52	91.51	91.78
				C (1)–Re (1)–N (5)	173.94	175.41	176.12
				C (2)–Re (1)–N (5)	93.81	93.30	93.24
				C (3)–Re (1)–N (5)	93.66	91.94	92.71
				N (5)–Re (1)–Cl (1)	83.63	82.92	84.30
				O (1)–C (1)–Re (1)	178.1	179.31	179.74
				O (2)–C (2)–Re (1)	178.4	178.24	177.47
				O (3)–C (3)–Re (1)	178.7	179.15	179.75

Table 9. The energy and molar absorption coefficients of the experimental absorption bands and the singlet electronic transitions calculated with the TD-DFT method and basis B1 for [Re (CO)$_3$(tp)$_2$Cl]

orbital excitations	Character	λ [nm]	E [eV]	f	Exp. λ [nm] (E[eV]) ε
H→L	d/π(Cl) →π*(tp)	365.6	3.39	0.0087	350.0.(3.54) 1520
H →L+1	d/ π (Cl) → π*(tp)	363.1	3.41	0.0121	
H-1 →L	d/ π (Cl) → π *(tp)	359.1	3.45	0.0037	
H-1 →L+1	d/ π (Cl) → π *(tp)	357.4	3.47	0.0040	
H-2 →L	d → π *(tp)	344.2	3.60	0.0108	
H-2 →L+1	d → π *(tp)	343.0	3.61	0.0080	
H-1 →L+4	d/ π (Cl) → π *(tp)	282.8	4.38	0.0221	269.8 (4.60) 13250
H →L+2	d/ π (Cl) → π *(tp)				
H-2 →L+2	d/ π (Cl) → π *(tp)	272.1	4.56	0.0474	
H-2 →L+3	d/ π (Cl) → π *(tp)	266.3	4.66	0.0353	
H-3 →L	π (Cl)/d → π *(tp)	258.1	4.80	0.0473	
H-2 →L+5	π (Cl)/d→ π *(tp)	257.6	4.81	0.0268	
H-3 →L	d→ π *(CO)/π *(tp)				
H-5 →L+1	π (Cl) → π *(tp)	243.6	5.09	0.0755	
H-6 →L		243.3	5.10	0.0776	
H →L+7		230.6	5.38	0.0278	227.6 (5.45) 25650

H-2 →L+6	π (Cl) → π *(tp) π (Cl)→ π *(tp) d → π *(tp) π (Cl) → π *(tp)/π*(CO) π (tp) → π *(tp)d/ π (Cl) → π *(tp)/π *(CO)	227.0	5.46	0.0510	
H →L+9		222.9	5.56	0.0292	
H-1 →L+9		216.3	5.73	0.0360	204.4 (6.07) 56000
H-10 →L+2		215.4	5.76	0.0285	
H →L+8		213.4	5.81	0.0256	
H-3 →L+4	π (Cl)/d→ π *(tp) d/ π (Cl) → π *(tp)/ π *(CO) π (Cl)/d→ π *(tp)	212.7	5.83	0.0996	

Table 10. The vertical excitation energy of the optimized lowest singlet and triplet states and bond lengths between Re and ligand atoms for [Re $(CO)_3(tp)_2Cl$] in basis B2

State	E (eV)	λ (nm)	Re (1)–C (1)	Re (1)–C (2)	Re (1)–C (3)	Re (1)–Cl (1)	Re (1)–N (1)	Re (1)–N (5)
S1	1.99	623.6	1.978	1.999	1.943	2.433	2.205	2.152
S2	2.16	574.0	1.980	1.995	1.951	2.428	2.165	2.212
S3	2.39	517.7	1.985	1.962	1.981	2.502	2.153	2.179
S4	2.40	516.2	1.972	1.991	1.962	2.431	2.174	2.189
S5	2.61	475.2	1.987	1.967	1.972	2.486	2.173	2.160
T1	1.83	677.3	1.984	1.975	1.947	2.466	2.200	2.120
T1	2.06	601.9	1.996	1.974	1.955	2.466	2.199	2.112
T1	—0.05	545.6	1.950	2.145	1.921	2.467	2.229	2.220
T2	2.10	590.4	1.997	1.998	1.934	2.420	2.176	2.200
T3	2.21	560.1	1.975	1.979	1.955	2.473	2.208	2.148
T4	2.37	523.0	1.978	1.993	1.954	2.429	2.174	2.188
T5	2.53	489.1	1.968	1.978	1.973	2.471	2.171	2.185

2.2.6. R_2SnCl_2 $(tp)_2$ compounds (R = Me, Et)

The two lowest energy structures were created using DFT calculations on $R_2SnCl_2(tp)_2$ molecules (R = Me, Et). **Table 11** depicts their key geometrical characteristics, relative energy, and computed DE values. As demonstrated in **Table 11**, the structure of the cis-Cl_2 isomer is more stable in gas than the trans-Cl_2 isomer for $Me_2SnCl_2(tp)_2$ and $Et_2SnCl_2(tp)_2$ compounds by kJ/mol. The preferred geometry is $Me_2SnCl_2(tp)_2$ _B, i.e., the all-trans geometry, and $Et_2SnCl_2(tp)_2$ A, i.e., the trans-diethyl, cis-Cl_2 geometry, based on a comparison of computed and observed nuclear quadrupole splitting values. In fact, there may be a preferred understanding of the structure of the compound Et2SnCl2$(tp)_2$, as displayed in **Table 12**, between the experimental DE, 3.45 mm s-1, and the computed worth relative to the majority stable structure, agreement between the experimental DE, 3.45 mm s-1, and that computed to $Et_2SnCl_2(tp)_2$ _B, 4. 10 mm s-1, as shown in **Table 13**. For the same structural environment, there is good agreement between the computed value of the C–Sn–C angle of $Et_2SnCl_2(tp)_2$A, 136.4o, and the one assessed by the point charge formalism, 141o [70, 71]. In the case of Me2Sn-Cl2$(tp)_2$, however, the desired structure would not be the most energetically stable in vacuo, i.e., $Me_2SnCl_2(tp)_2$A, since $Me_2SnCl_2(tp)_2$ B has a considerably better agreement between the experimental and predicted DE, i.e., 4.16- and 4.15-mm s-1, respectively (see **Tables 11** and **12**).

Table 11. ^{119}Sn Mo¨ssbauer parameters of diorganotin (IV) chlorides and their tp and dmtp adducts

	Compound	b (mm s^{-1})	ΔE[c] (mm s—1)	I[d] (mm s^{-1})	Area (mms 1)
1	$Me_2SnCl_2(tp)_2$	1.41	4.16	0.86	0.0780
	at 294 K	1.38	4.11	0.84	0.0075
	MeOH sol., 0.1 M	1.38	4.10	0.82	
2	$Et_2SnCl_2(tp)_2$	1.51	3.45	0.80	
	MeOH sol., 0.1 M	1.56	4.02	0.82	
3	$Me_2SnCl_2(dmtp)_2$	1.44	4.00	0.81	
	MeOH sol., 0.1 M	1.41	3.91	0.82	
4	$Et_2SnCl_2(dmtp)_2$	1.59	4.02	0.77	
	MeOH sol., 0.1 M	1.55	3.91	0.79	
5	n-Bu_2SnCl_2(dmtp)	1.45	3.24	0.79	
	MeOH sol., 0.1 M	1.54	4.01	0.84	
6	Ph_2SnCl_2(dmtp)	1.26	2.89	0.84	
	MeOH sol., 0.1 M	1.28	3.65	0.84	
	Me_2SnCl_2, MeOH sol., 0.1 M	1.41	3.92	0.82	
	Et_2SnCl_2, MeOH sol., 0.1 M	1.55	4.07	0.85	
	n-Bu_2SnCl_2, MeOH sol., 0.1 M	1.55	3.90	0.87	
	Ph_2SnCl_2, MeOH sol., 0.1 M	1.32	3.67	0.93	

"a" In the solid state and at liquid-nitrogen temperature, unless otherwise specified.
"b" Isomer shift with respect to room-temperature $CaSnO_3$.
"c" Nuclear quadrupole splitting.
"d" Full width at half-height of the resonant peaks.

Table 12. Geometrical parameters (bond distances, in A°, and angles, in degrees), their relative energy and calculated nuclear quadrupole splitting values calculated at DFT level (see text) for the compounds

tp		$Me_2SnCl_2(tp)_2$	$Me_2SnCl_2(tp)_2$	$Et_2SnCl_2(tp)_2$	$Et_2SnCl_2(tp)_2$
		A	B	A	B
Sn–N (3)	–	3.008	2.470	2.992	2.423
Sn–N (3^0)	–	3.028	2.470	3.120	2.605
Sn–C	–	2.157	2.179	2.179	2.201
Sn–C^0	–	2.161	2.166	2.182	2.190
Sn–Cl	–	2.452	2.548	2.452	2.553
Sn–Cl^0	–	2.440	2.630	2.450	2.645
N (1)–C (2)	1.340	1.336	1.330	1.337	1.331
C (2)–N (3)	1.353	1.356	1.360	1.356	1.360
N (3)–C (3)	1.335	1.337	1.343	1.338	1.342
C (3)–N (8)	1.405	1.399	1.393	1.399	1.393
C (3)–N (4)	1.348	1.345	1.340	1.345	1.340
N (4)–C (5)	1.322	1.323	1.323	1.322	1.323
C (5)–C (6)	1.425	1.423	1.423	1.423	1.423
C (6)–C (7)	1.374	1.374	1.374	1.374	1.374
C (7)–N (8)	1.357	1.357	1.358	1.357	1.358
N (1)–N (8)	1.358	1.359	1.363	1.359	1.363
C–Sn–C^0	–	135.5	179.5	136.4	171.1
N (3)–Sn–N (3^0)	–	106.1	168.6	103.5	167.4
Cl–Sn–Cl^0	–	97.2	176.6	97.4	168.3
N (3)–Sn–Cl	–	78.7	95.5	78.8	87.2
N (3)–Sn–Cl^0	–	175.4	84.4	175.5	81.5
N (3^0)–Sn–Cl	–	175.2	95.6	177.6	105.5

N (3^{0})–Sn–Cl0	–	78.1	84.4	80.2	85.9
N (1)–C (2)–N (3)	117.1	116.6	115.7	116.6	115.7
C (2)–N (3)–C (3)	103.0	103.2	104.2	103.2	104.1
N (3)–C (3)–N (8)	108.5	108.3	107.4	108.3	107.5
C (3)–N (4)–C (5)	116.4	116.3	116.1	116.3	116.1
N (4)–C (5)–C (6)	124.4	124.3	124.2	124.2	124.2
C (5)–C (6)–C (7)	118.6	118.6	118.6	118.6	118.6
C (6)–C (7)–N (8)	116.9	116.9	116.9	116.9	116.9
C (7)–N (8)–C (3)	122.1	122.0	121.7	122.0	121.7
Energy (kJ/mol)	–	0.0	21.3	0.0	22.4
DE_{calcd} (mm s^{-1})	–	2.82	4.15	2.89	4.10

2.2.7. Triazolo[1,5-a] pyrimidine derivatives

Optimization of triazolo[1,5-*a*] pyrimidine derivatives in the gas phase using DFT at the B3LYP/6-311G (df, pd) level of theory. **Table 13** [72] illustrates the EHOMO, ELUMO, energy gap Eg, and dipole moment of all derivatives. **Table 14** shows the actual and theoretical electronic absorption spectra of chemical (**45**) in Dioxane and DMF. The theoretical gas phase transitions of the different subsystems a, b, and c were also estimated and presented in **Table 15** using TD-B3LYP/6-311G (d, p). Inserting a NO_2 group in position X and a F atom in position Y in Ph-X and Ph-Y of compound (**46**) yields compound (**46**) (**45**). **Table 16** shows the experimental and theoretical electronic absorption spectra of compound (**46**) in Dioxane and DMF, just as compound (**45**). By placing the F atom in Ph-Y and the OCH3 group in position X, compound (**47**) is formed (**46**). The actual and theoretical electronic absorption spectra of compound (**47**) in Dioxane and DMF are displayed in **Table 17**. **Table 18** shows the experimental and theoretical electronic absorption spectra of compound (**48**) in Dioxane and DMF, which was made by replacing the F atom in position X of compound (**46**) to make compound (**48**). The synthesis of compound (**48**) is achieved by replacing the F atom at position X with a Br atom (**49**). The actual and theoretical electronic absorption spectra of compound (**49**) in Dioxane and DMF are reported in **Table 19**. The synthesis of compound (**46**), when the CH3 group is inserted in position X, is compound (**46**) and (**50**). The actual and theoretical electronic absorption spectra of compound (**50**) in Dioxane and DMF are shown in **Table 20**. The -isoelectronic compound (**51**) is made by replacing the F atom with the OCH_3 group of compounds (**47**). In dioxane and DMF [73], **Table 21** illustrates the experimental and theoretical electronic absorption data of compound (**51**).

Table 13. Theoretical calculation of total energy, E_{HOMO}, E_{LUMO}, Energy gap (Eg) and dipole moment of compounds (**45- 51**), calculated at B3LYP/6-311G (df, pd) in gas phase

G.S. Properties	**45**	**46**	**47**	**48**	**49**	**50**	**51**
E_T (au)	-875.476663	-1179.305339	-1089.302333	-1074.011424	-3548.288468	-1014.072869	-1089.303477
E_{HOMO} (eV)^{a} (eV)^{a}	-5.803	-6.230	-5.806	-5.971	-6.021	-5.844	-5.764
E_{LUMO} (eV)^{b}	-1.277	-2.662	-1.234	-1.359	-1.423	-1.253	-1.081
E_g (eV)	4.527	3.567	4.572	4.612	4.597	4.591	4.683
μ (debye)	4.00	5.36	3.43	2.85	3.05	2.88	5.63
D (5-6-10-15) ^{c}	63.129	48.855	68.854	71.672	69.514	66.096	73.934

D (9-8-16-17) [c]	36.513	37.991	36.295	36.843	36.268	36.720	36.235

[a] I.E., = - *EHOMO*
[b] E.A. = - *ELUMO*
[c]For numbering system.

Table 14. The experimental and theoretical electronic absorption spectra of compound (**45**) in dioxane and DMF

Ex. states	Theoretical												Experimental		Assig.
	Gas phase				Dioxane				DMF				Dioxane	DMF	
	Config.	Coeff.	f	λ, nm	Config.	Coeff.	f	λ, nm	Config.	Coeff.	f	λ, nm	λmax, nm	λmax, nm	
S1	72 -> 73	0.700	0.0555	313.5	72 -> 73	0.701	0.0841	310.2	72 -> 73	0.699	0.0933	305.9	308.0	293.0	Electron delocal.
S2	72 -> 74	0.699	0.0019	282.1	72 -> 74	0.696	0.0031	276.1	72 -> 74 72 -> 75	0.675 - 0.175	0.0009	270.6			
S3	72 -> 75	0.701	0.0011	269.1	72 -> 75	0.702	0.0023	268.6	72 -> 74 72 -> 75	0.162 0.675	0.0061	269.4			
S4	72 -> 76	0.697	0.0048	259.6	72 -> 76	0.696	0.0062	258.6	72 -> 76	0.696	0.0051	258.7			
S5	69 -> 73 71 -> 73	0.113 0.671	0.2468	248.0	71 -> 73	0.678	0.3758	246.8	70 -> 73 71 -> 73	- 0.112 0.669	0.4037	244.1	262.0	266.0	Electron delocal.
S6	65 -> 74 68 -> 73 69 -> 74 70 -> 74 71 -> 74	- 0.124 0.486 0.145 0.197 - 0.412	0.0007	240.3	65 -> 74 68 -> 73 70 -> 74 71 -> 74 72 -> 74	0.113 0.514 0.202 -0.387 -0.112	0.0035	239.5	68 -> 73 70 -> 74 71 -> 74 71 -> 75 72 -> 74	0.534 - 0.140 - 0.325 - 0.183 0.121	0.0088	238.8			

Table15. Theoretical vertical excitations of compound (**45**) and its subsystems calculated at TD-B3LYP/6-311G (d, p) in gas phase

Single point vertical excitation	a	b	c	Compound **45**
1	250.0	263.4	281.7	259.6
2		274.9	308.1	269.1
3				282.1
4				313.5

Table16. Experimental and theoretical UV spectra of compound (**46**), calculated at TD-B3LYP/6-311G (d, p)

Ex. states	Theoretical			Experimental	Assig.
	Gas phase	Dioxane	DMF	Dioxane DM	

	config. vv vConfig.	Coeff.	f	λ, nm	confing, an. fffffConfig.	Coeff.	f	λ, nm	confing, s. nfig.	Coeff.	f	λ, nm	λmax, nm	λmax, nm	
S1	87 - -> 88	0.704	0.0210	407.9	87 - -> 88	0.705	0.0266	431.4	87 - > 88	0.705	0.0267	461.9			
S2	80 - -> 88 81- -> 88 81- -> 92	0.129 0.679 - 0.119	0.0000	323.4	79 - > 88 80 - > 88 80 - > 92	0.307 0.620 - 0.100	0.0000	322.2	86 - > 88	0.704	0.0463	333.9			
S3	86 - -> 88	0.700	0.0490	304.1	86 - > 88	0.704	0.0592	317.7	79 - > 88 79 - > 92	0.694 - 0.102	0.0001	320.8	319.0	322.0	CT-band
S4	87- -> 89	0.690	0.0691	299.4	87 - > 89	0.691	0.0935	299.4	83 - > 88 84 - > 88 87 - > 89 87 - > 90	0.137 - 0.167 0.655 - 0.120	0.1033	298.8			
S5	87 - -> 90	0.699	0.0048	287.3	83 - > 88 85 - > 88 85 - > 91 87 - > 91	0.587 - 0.290 - 0.104 - 0.174	0.0194	285.9	83 - > 88 84 - > 88 87 - > 89	0.586 - 0.297 - 0.209	0.0338	295.3			
S6	78 - -> 88 78- -> 92	0.689 - 0.114	0.0002	286.3	78 - > 88 78 - > 92	0.687 - 0.105	0.0014	283.5	78 - > 88 83 - > 88 84 - > 88 87 - > 90	- 0.104 0.251 0.538 - 0.351	0.2273	283.3			
S7	83- -> 88 84- -> 88 85 - -> 88 87 - -> 91	0.159 0.409 - 0.139 0.515	0.0064	279.0	87 - > 90	0.691	0.0103	282.7	85 - > 88 87 - > 90 87 - > 91	0.582 0.173 0.349	0.0036	280.4			
S8	83 - > 88 84 - > 88 85 - > 88 87 - > 91	- 0.123 - 0.388 0.309 0.462	0.0114	275.2	85 -> 88 87 -> 91	- 0.306 0.625	0.0357	278.9	78 -> 88 87 -> 90	0.630 - 0.262	0.0007	279.9			
S9	84 - > 88 85 - > 88 87 - > 91	0.318 0.604 0.108	0.1939	268.0	83 -> 88 85 -> 88 87 -> 91	0.338 0.549 0.241	0.2452	275.0	78 -> 88 83 -> 88 84 -> 88 85 -> 88 87 -> 89 87 -> 90	0.271 0.225 0.279 - 0.158 0.102 0.498	0.0718	279.5	286.0	287.0	Electron delocal.

Table17. Experimental and theoretical UV spectra of compound (**47**), calculated at TD-B3LYP/6-311G (d, p)

Ex. States	Theoretical												Experimental		
	Gas phase				Dioxane				DMF				Dioxane	DMF	Assig.
	Config.	Coeff.	f	λ, nm	Config.	Coeff.	f	λ_{max}, nm	Config.	Coeff.	f	λ_{max}, nm	λ_{max}, nm	λ_{max}, nm	
S1	84 - > 85 84 -> 85	0.696	0.0692	309.4	84 - >85	0.698	0.1036	306.5	84 - > 85	0.697	0.1179	301.7	328.0	327.0	Electron delocal.
S2	84 - > 86	0.696	0.0064	300.1	84 - > 86	0.696	0.0095	293.3	84 - > 86	0.695	0.0116	285.4	297.0	295.0	CT-band
S3	83 - > 85	0.698	0.0755	276.6	83 - > 85	0.697	0.0965	273.8	83 - > 85 84 - > 87	-0.341 0.609	0.0242	268.9	275.0	273.0	CT-band
S4	84 - > 87	0.700	0.0021	266.3	84 - > 87	0.700	0.0034	266.5	83 - > 85 84 - > 87	0.605 0.347	0.0813	268.3			
S5	83 - > 86	0.699	0.0012	258.5	83 - > 86	0.695	0.0020	253.0	83 - > 87 84 - > 88	0.253 0.638	0.0094	250.9			
S6	83 - > 87 84 - > 88	0.255 0.637	0.0065	249.9	83 - > 87 84 - > 88	0.282 0.625	0.0091	250.1	81 - > 85 81 - > 88 83 - > 86 83 - > 87 83 - > 88 84 - > 88	-0.115 0.160 -0.394 0.459 0.116 -0.215	0.0352	245.7			
S7	81 - > 85 81 - > 88 83 - > 87 83 - > 88 84 - > 88	0.180 0.211 0.556 0.152 0.263	0.0225	244.9	81 - > 85 81 - > 88 83 - > 87 83 -> 88 84 - > 88	-0.152 0.195 0.556 0.145 -0.290	0.0352	245.3	80 - > 85 81 - > 88 82 - > 86 83 - > 86 83 - > 87 84 - > 88	-0.113 0.110 -0.137 0.545 0.341 -0.136	0.0091	244.9	255.0		Electron delocal.

Table 18. Experimental and theoretical UV spectra of compound (**48**), calculated at TD-B3LYP/6-311G (d, p)

	Theoretical												Experimental		Assig.
Ex. states	Gas phase				Dioxane				DMF				Dioxane	DMF	
	Config.	Coeff.	f	λ, nm	Config.	Coeff.	f	λ, nm	Config.	Coeff.	f	λ, nm	λ_{max}, nm	λ_{max}nm,	
S1	80 -> 81	0.698	0.0518	307.3	8 -> 81	0.699	0.0834	305.3	80 ->81	0.698	0.0932	302.3	319.0	319.0	Electron delocal.
S2	80 -> 82	0.700	0.0044	295.3	80 -> 82	0.700	0.0069	288.9	80 ->82	0.698	0.0088	282.6			
S3	80 -> 83	0.702	0.0001	273.5	80 -> 83	0.702	0.0003	274.4	80 ->83	0.701	0.0003	276.4			
S4	80 -> 84	0.697	0.0020	259.4	80 -> 84	0.695	0.0032	258.3	80 ->84	0.692	0.0034	258.9			
S5	78 -> 81	0.129 0.672	0.2129	249.8	79 -> 81	0.675	0.3458	248.5	78 ->81 79 ->81	-0.131 0.663	0.3833	245.7	263.0	267.0	Electron delocal.

	79 -> 81														
S6	75 -> 81 78 -> 82 79 -> 82	0.332 -0.318 0.517	0.0079	244.2	76 -> 81 78 -> 82 79 -> 82	0.358 0.287 0.513	0.0085	242.0	76 ->81 78 ->82 79 ->	0.391 0.222 0.514	0.0048	239.7			

Table 19. Experimental and theoretical UV spectra of compound (49), calculated at TD-B3LYP/6-311G (d, p)

Ex. states	Theoretical												Experimental		Assig.
	Gas phase				Dioxane				DMF				Dioxane	DM	
	Config.	Coeff.	f	λ, nm	Config.	Coeff.	f	λ, nm	Config.	Coeff.	f	λ, nm	λ_{max}, nm	λ_{max}, nm	
S1	80 - > 81	0.697	0.0618	309.2	93 -> 94	0.697	0.0926	308.1	93 -> 94	0.695	0.1009	306.6	317.0	314.0	Electron delocal.
S2	80 - > 82	0.700	0.0043	293.7	93 -> 95	0.700	0.0062	287.8	93 -> 95	0.702	0.0019	284.1			
S3	80 - > 83	0.703	0.0013	279.5	93 -> 96	0.702	0.0034	280.9	93 -> 96	0.697	0.0116	281.2			
S4	80 - > 84	0.698	0.0010	268.1	93 -> 97	0.697	0.0022	267.5	93 -> 97	0.694	0.0048	267.5			
S5	78 - > 81 79 - > 81	0.104 0.673	0.1976	254.2	90 -> 96 92 -> 94	0.105 0.670	0.3328	251.9	90 -> 95 92 -> 94	0.104 0.655	0.3786	248.8	268.0	268.0	Electron delocal.

Table 20. Experimental and theoretical UV spectra of compound (**50**), calculated at TD-B3LYP/6-311G (d, p)

Ex. states	Theoretical												Experimental		Assig.
	Gasphase				Dioxane				DMF				Dioxane	DMF	
	Config.	Coeff.	f	λ, nm	Config.	Coeff.	f	λ, nm	Config.	Coeff.	f	λ, nm	λ_{max}, nm	λ_{max}, nm	
S1	80 - > 81 80 -> 81	0.698	0.0599	308.8	80 -> 81	0.699	0.0924	306.9	80 -> 81	0.698	0.1035	303.1	313.0	291.0	Electron delocal.
S2	80 - > 82	0.700	0.0048	298.4	80 -> 82	0.700	0.0075	291.7	80 -> 82	0.698	0.0095	284.4			
S3	80 - > 83	0.703	0.0009	267.7	80 -> 83 80 -> 84	0.694 0.114	0.0017	261.9	80 -> 83 80 -> 84	0.695 0.108	0.0020	263.1			

S4	79 - > 81 80 - > 84	0.280 0.632	0.0261	255.2	80 - > 83 80 - > 84	-0.113 0.684	0.0056	257.9	80 - > 83 80 - > 84	-0.108 0.684	0.0039	258.1			
S5	79 - > 81 80 - > 84	0.627 - 0.290	0.1552	254.0	79 - > 81	0.685	0.2692	253.0	79 - > 81	0.679	0.2969	249.6	267.0	268.0	Electron delocal.

Table 21. Experimental and theoretical UV spectra of compound **51**, calculated at TD-B3LYP/6-311G (d, p)

Ex. states	Theoretical											Experimental			Assig.
	Gas phase				Dioxane				DMF			Dioxane		DMF	
	Confi.	Coeff.	f	λ, nm	Config.	Coeff.	f	λ, nm	Config.	Coeff.	f	λ, nm	$\lambda_{max,}$ nm	$\lambda_{max,}$ nm	
S1	84 - > 85	0.687	0.0519	301.9	84 - > 85	0.690	0.0903	300.8	83 - > 85 84 - > 85	0.108 0.688	0.1168	299.7	330.0	331.0	Electron delocal.
S2	84 - > 86	0.692	0.0176	286.4	84 - > 86	0.688	0.0243	281.4	84 - > 86	0.694	0.0015	281.9	274.0	288.0	CT-band
S3	84 - > 87	0.697	0.0009	278.9	84 - > 87	0.693	0.0016	280.0	81 - > 85 84 - > 87	-0.123 0.688	0.0270	277.0			
S4	83 - > 85 84 - > 88	0.163 0.677	0.0032	262.4	83 - > 85 84 - > 88	-0.284 0.635	0.0256	261.7	83 - > 85 84 - > 88	-0.485 0.498	0.1323	261.0			
S5	83 - > 85 83 - > 86 84 - > 88	0.632 -0.179 -0.140	0.4241	254.7	83 - > 85 84 - > 85 84 - > 88	0.623 0.117 0.268	0.5743	257.7	83 - > 85 84 - > 85 84 - > 88	0.485- 0.136 0.471	0.4415	257.9	254.0	267.0	Electron delocal.
S6	80 - > 85 83 - > 85 83 - > 86	-0.257 0.189 0.603	0.1102	250.7	80 - > 85 83 - > 86	-0.261 0.629	0.0369		81 - > 85 83 - > 87	0.271 0.626	0.0156	246.9			

2.2.8. Triazolopyrimidine derivatives

Quantum and molecular mechanics calculations indicated that the Inhibition Efficiency was related to quantum chemical parameters. The experimental Inhibition Efficiency was found to be close to that of the theoretical study. In terms of inhibitory effectiveness, (Pyrimidine thione) (**53**) surpasses Pyrimidinones, according to the findings (IE). Inhibition efficiency for triazolopyrimidine derivatives as corrosion inhibitors for steel in acidic media has been reported as Eexp (percent) based on the approach of weight loss for compounds (**52–53**). As indicated in **Table 22**, compound **53** has

the greatest EHOMO value, which is compatible with the experimental percent inhibition efficiency data, suggesting that triazolopyrimidine thione (**53**) is a better inhibitor than pyrimidinones. The addition of a sulfur atom to thione boosts efficiency when compared to the oxygen counterpart. The capacity to accept electrons is indicated by the ELUMO. As a result, the lower the ELUMO value, the better the chances of the molecule receiving electrons. In **Table 22** and **Tables 23**, ELUMO has the lowest value (**53**). All the compounds discussed in this section are illustrated in **Scheme 16**. The correlation coefficients and degree of linearity between DFT-calculated quantum chemical parameters and experimental inhibitory efficacy of the Triazolo pyrimidines studied are depicted in **Table 24**. The theoretical inhibitory efficiencies and quantum chemical descriptors for the Triazolopyrimidine derivatives investigated using the AM1 model are shown in **Table 25** and **Table 26** [74, 75]. A comparison of the inhibitory efficiency of several Triazolopyrimidine derivatives demonstrates that orbital energies (EHOMO and ELUMO), Energy band gap (ELUMO-EHOMO), Dipole moment (μ), Log P, Polarizability, Softness(S), and Hardness(η) are all intricately connected to their inhibition impact. With increasing EHOMO, lowering ELUMO, reducing ELUMO-EHOMO, rising Dipole moment, raising Log P, increasing Polarizability, increasing Softness, and decreasing Hardness, the inhibitory efficacy of the Triazolopyrimidine derivatives improves. As evidenced by the experimental data, (**53**) (Pyrimidine thione) had a higher Inhibition Efficiency (IE) than Pyrimidinones. A high significant coefficient of determination (R2 =0.804) was determined between experimental and inhibitory efficiency.

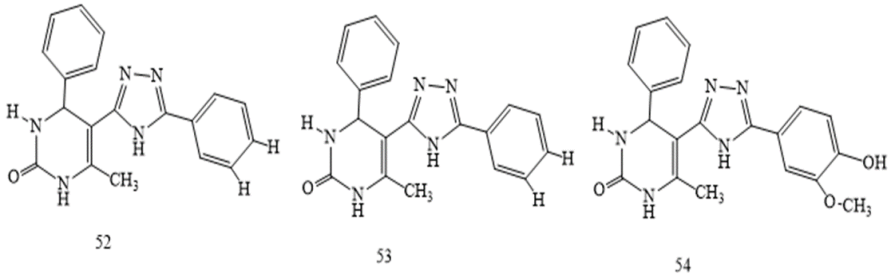

Scheme 16. (**52-54**) studied compounds

Table 22. Quantum chemical parameters of triazolopyrimidine derivatives using AM1 method

Quantum chemical parameters	52	53	54
E_{Homo} (eV)	- 8.56	- 8.59	- 8.46
E_{Lumo} (eV)	- 0.51	- 0.78	- 0.53
$E_{Lumo} - E_{Homo}$ (eV)	8.05	7.81	7.93
Dipole moment (μ)	5.04	5.95	2.89
Log P	2.29	3.44	1.78
Polarizability	66.76	67.57	69.59
E_{exp} (%)	96.00	99.72	93.79

Table 23. Quantum chemical parameters of triazolopyrimidine derivatives using DFT method

Quantum chemical parameters	52	53	54
E_{Homo} (eV)	- 5.47	-5.22	-5.23
E_{Lumo} (eV)	- 1.13	- 1.47	- 0.99
$E_{Lumo} - E_{Homo}$ (eV)	4.34	4.05	4.24
Dipole moment (μ)	4.92	5.94	3.39
Log P	0.70	1.84	-1.36
Polarizability	67.56	68.43	70.35
E_{exp} (%)	96.00	99.72	93.79

Table 24. Correlation coefficients, r (degree of linearity, R^2) between quantum chemical parameters and experimental inhibition efficiencies of the studied triazolo pyrimidines

Quantum parameter	Correlation Coefficient(r)	Degree of linearity (R^2)
E_{HOMO}	0.901	0.812
E_{LUMO}	0.903	0.815
$E_{LUMO-HOMO}$	0.621	0.385
Dipole moment	0.930	0.865
Log P	0.997	0.994
Polarizability	0.581	0.337

Table 25. Theoretical inhibition efficiencies of the studied triazolopyrimidine obtained from AM1 model

Concentration	IE_{Theor} (%)	IE_{Exp} (%)	IE_{Theor} (%)	IE_{Exp} (%)	IE_{Theor} (%)	IE_{Exp} (%)
0.02	67.29	50.08	68.42	66.39	66.21	51.09
0.04	80.44	65.94	81.25	82.29	79.67	68.18
0.06	86.05	73.77	86.67	89.18	85.46	75.44
0.08	89.16	76.86	89.66	96.22	88.68	80.91
0.10	91.14	80.02	91.55	98.75	90.74	82.29
0.15	93.91	83.31	94.20	99.15	93.63	86.69
0.25	96.26	87.40	96.44	99.16	96.08	89.92
0.50	98.09	93.81	98.19	99.43	98.00	92.62
1.00	99.04	96.00	99.09	99.72	98.99	93.79

Table 26. Calculated quantum chemical descriptors for the studied triazolopyrimidine derivatives using AM1 model

Inhibitor	E_N/ eV	$E_{(N-1)}$/eV	$E_{(N+1)}$/eV	IP/eV	EA/eV	S/eV [1]
Mol 1	4.62	11.95	2.82	7.33	1.80	0.1808
Mol 2	6.98	14.33	4.97	7.35	2.01	0.1873
Mol 3	1.06	8.32	-0.84	7.26	1.90	0.1866

2.2.9. Compounds (57a-e) and (60a, g, h)

The relative Gibbs free energies (ΔG^{298}), dipole moments (μ), and Boltzmann populations (x) of tautomer A-D compounds **(57a-e)** and **(60 a,g,h)** which calculated by the DFT method at B3LYP/6-311++G(2d,2p) in the gas, DMSO, and water phases [76]. All results obtained in this study are indicated in **Table 27**.

Table 27. Relative Gibbs free energies ΔG^{298} (kcal/mol), [a] dipole moments μ(D), and relative populations x (%) of tautomer A-D of model compounds (**57**) and (**60**) at 48 °C calculated by the B3LYP/6-311++G(2d,2p) method"

Tautomer	ΔG^{298}	μ	x	Tautomer	ΔG^{298}	μ	x
Gas (ε=1)							
57A	15.63	14.49	0.00	60A	18.74	13.41	0.00
57B	0	1.98	100.00	60B	0	0.26	100.00
57C	12.22	6.95	0.00	60C	14.06	5.31	0.00
57D	9.74	1.53	0.00	60D	9.56	3.31	0.00
Dimethyl sulfoxide (ε = 46.7)							
57A	0	21.21	97.62	60A	1.58	19.99	6.46
57B	2.20	2.45	2.38	60B	0	0.31	93.54

57C	10.21	10.16	0.00	60C	9.98	8.34	0.00
54D	10.82	2.86	0.00	60D	8.41	5.21	0.00
Water (ε = 78.4)							
57A	0	21.37	98.21	60A	0.74	20.18	22.42
57B	2.37	2.45	1.79	60B	0	0.35	77.58
57C	10.30	10.24	0.00	60C	9.87	8.42	0.00
57D	10.96	2.89	0.00	60D	8.31	5.24	0.00

*2.2.10. Compounds **66-68***

The Gibbs free energy (G^{298}) for each tautomer was calculated using DFT techniques to optimize the geometry of (**66-68**) compounds. The 67A molecule is the most stable tautomeric, according to our findings. The following relationship was used to calculate the equilibrium compositions of mixes of isomers using conventional Gibbs free energy calculations: $\Delta G = -RT \ln K$. The values of ΔG^{298} and the relative concentrations of the isomers in aqueous solutions. These factors had no effect in vacuum or DMSO solutions on Molecules (67A) and (**68**), which are much more stable isomers in the relevant equilibrium. The experimentally observed kinetic product 16n to thermodynamic product 11n rearrangement is in good accord. In cyclo condensations, the production of isomers **66 and 67** appears to be predicted [77]. Although in the case of R = H, the model cations **67** are somewhat more stable than (**66**), the presence of bulky substituents in the actual molecules moves the equilibrium to the side of isomers (**66**), as observed in the case of R = Ph.

2.2.11. Amino [1,2,4] triazolo- [1,5-a] pyrimidines (73a,74a,75a)

Model compounds for theoretical reactivity assessment using DFT techniques were 2-amino [1,2,4] triazolo- [**1,5-*a***] pyrimidines (**73a**,**74a**,**75a**). The global nucleophilicity of amino triazolo pyrimidines increases with increased pyrimidine ring saturation, according to most reactivity indices, as indicated in **Table 28**. The aromatic compound (**75a**) depicts a greater rise in nucleophilicity than the dihydro derivative (**74a**), whereas the nucleophilicity of compounds (**73a**) and (**74a**) was virtually identical. During frontier-controlled interactions, the Fukui functions f_k^- reflect the reactivity of molecules. The N-1 atom and amino group should be the most nucleophilic sites in compounds (**73–75a**) towards soft electrophiles, according to the data in **Table 29**, whereas the *N*-4 atom should be the most nucleophilic site in compounds (**73a**) and (**74a**). When a polar solvent (water) is compared to a nonpolar medium (gas), the reactivity of the N-1 atom should rise, whilst the reactivity of the amino group should decrease in compounds (**73a**) and (**74a**) but increase in compound (**75a**). In aqueous solution, the relative nucleophilicity of the N-4 atom in molecules (**73a**) and (**74a**) is also somewhat greater. As demonstrated in **Scheme 17. Table 29** [78] lists all of the compounds examined in this section.

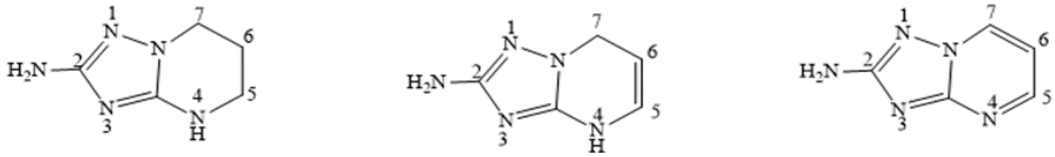

74a 73a 75a

Scheme 17. Amino [1,2,4] triazolo- [1,5-*a*] pyrimidines (**73a**,**74a**,**75a**) studied compounds

Table 28. The global reactivity indices of compounds (**73a**, **74a**, **75a**), calculated at the DFT B3LYP/6-311++G(2d,2p) level of theory in gas phase and aqueous solution

Global reactivity	Gas phase			Aqueous solution		
indices	**73a**	**74a 74a**	**75a**	**73a**	**74a**	**75a**
ε_{HOMO}, eV	–5.80	–5.551	–6.539	–5.769	–5.697	–6.653
ε_{LUMO}, eV	–0.491	–0.456	–1.896	–0.227	–0.290	–1.944

μ, a. u.	–0.110	–0.110	–0.155	–0.110	–0.110	–0.158
η, a. u.	0.092	0.094	0.085	0.102	0.099	0.087
S, a. u. 1	5.454	5.341	5.861	4.911	5.033	5.779
Nu (1), a. u. 1	15.23	15.37	7.10	16.78	16.42	6.94
Nu (2), a. u. 1	9.04	9.00	5.91	9.06	9.07	5.79
Nu (3), eV	4.02	3.94	2.96	3.73	3.80	2.84

Table 29. The Fukui functions fk^- for electrophilic attack and local nucleophilicity values* $Nuk^{(i)}$ for compounds (**73a**,**74a**, **75a**) calculated at the DFT B3LYP/6-311++G(2d,2p) level of theory in gas phase and aqueous solution

R. site (*k*)	Gas phase				Aqueous solution			
	fk^-	$Nuk^{(1)}$, a.u.−1	$Nuk^{(2)}$, a.u.−1	$Nuk^{(3)}$, eV	fk^-	$Nu^{(1)}$, a.u.−1	$Nuk^{(2)}$), a.u.−1	$Nuk^{(3)}$, eV
Compound 73a								
N-1	0.225	3.43	2.03	0.90	0.239	4.01	2.17	0.89
NH2	0.162	2.47	1.46	0.65	0.147	2.47	1.33	0.55
N-3	0.059	0.90	0.53	0.24	0.069	1.16	0.63	0.26
N-4	0.138	2.10	1.25	0.55	0.156	2.62	1.41	0.58
Compound 74a								
N-1	0.181	2.78	1.63	0.71	0.173	2.84	1.57	0.66
NH2	0.127	1.95	1.14	0.50	0.089	1.46	0.81	0.34
N-3	0.062	0.95	0.56	0.24	0.064	1.05	0.58	0.24
N-4	0.128	1.97	1.15	0.50	0.160	2.63	1.45	0.61
Compound 75a								
N-1	0.158	1.12	0.93	0.47	0.187	1.30	1.08	0.53
NH2	0.252	1.79	1.49	0.75	0.280	1.94	1.62	0.80
N-3	0.087	0.62	0.51	0.26	0.090	0.62	0.52	0.26
N-4	0.048	0.34	0.28	0.14	0.040	0.28	0.23	0.11

* Local nucleophilicity values were calculated according to the equation $Nuk^{(i)} = Nu^{(i)} \cdot fk^-$.

2.2.12. System (101) with R =C_nH_{2n}+1

2.2.12.1. A-Rearrangement in an acidic medium

As indicated in **Table 30**, DFT calculations were used to calculate the electron chemical potentials, chemical harnesses, and global electrophilicity for system (**101**) with R =CnH2n+1, where n = 0, 1, 2, 3, or 4, which are used as efficient static descriptors for the prediction of the reactivity of this system. This is consistent with the results of experiments on compound (98a) isomerization in acidic environments. The simulations also demonstrated that the interaction of (101) with such an electrophile is controlled by charges on atoms at long distances, whilst the reaction is controlled by the HOMO of the substrate at small distances [79, 80]. The contributions of the substrate's pz-AO to HOMO and HOMO are depicted in **Table 31**. (LUMO). The relative energies of the seven cationic adducts, as well as the lengths of the C (5)-N (4) link broken during recyclization, are shown in **Table 32**. In terms of the polarizable continuum model, **Table 33** estimated and summarized the solvation effects in the acid catalyzed rearrangement (PCM). Potential energy surface for proton-catalyzed rearrangements (**103**, **108**) in the gas phase (solid line) and in solution (dashed line) or is the reaction coordinate is provided in **Scheme 18**, and the structures of these compounds are illustrated in **Scheme 19**.

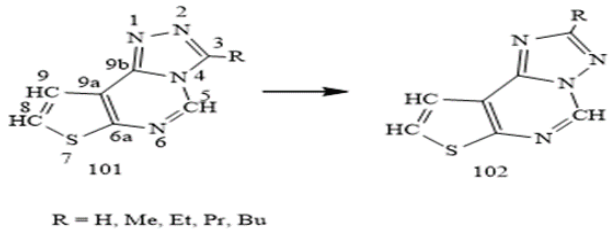

Scheme 18 Global electrophilicity for system (**101**)

Table 30. Electron chemical potentials (μ), the chemical harnesses (ŋ), and the global electrophilicity indices (ω) for system (101) with R = H, Me, Et, Pr, and Bu

R	-μ	ŋ	ω
H	4.1216	4.5626	1.8616
Me	3.9752	4.4732	1.7663
Et	3.9512	4.4684	1.7470
Pr	3.9423	4.4678	1.7392
Bu	3.9311	4.4510	1.7360

Table 31. Contributions of pz-AO to the frontier MO of system (101) with R = H, Me, Et, Pr, and Bu

Atom	HOMO					LUMO				
	H	Me	Et	Pr	Bu	H	Me	Et	Pr	Bu
N (1)	+0.21	+0.22	+0.22	+0.21	+0.21	–0.04	–0.04	–0.04	–0.04	–0.04
N (2)	–0.03	–0.06	–0.06	–0.06	–0.06	+0.16	+0.16	+0.15	+0.15	+0.15
C (3)	+0.19	+0.18	+0.18	+0.17	+0.17	–0.07	–0.07	–0.07	–0.07	–0.07
N (4)	–0.05	–0.07	–0.07	–0.07	–0.06	–0.15	–0.15	–0.15	–0.15	–0.14
C (5)	+0.16	+0.16	+0.16	+0.16	+0.16	+0.40	+0.41	+0.41	+0.41	+0.42
N (6)	+0.08	+0.07	+0.08	+0.08	+0.08	–0.24	–0.24	–0.24	–0.23	–0.23
C(6a)	–0.22	–0.21	–0.21	–0.21	–0.2	–0.20	–0.21	–0.21	–0.22	–0.22
S (7)	+0.08	+0.11	+0.12	+0.14	+0.16	+0.24	+0.23	+0.23	+0.23	+0.23
C (8)	+0.19	+0.17	+0.17	+0.16	+0.16	–0.29	–0.29	–0.29	–0.28	–0.28
C (9)	+0.05	+0.03	+0.02	+0.02	+0.02	+0.08	+0.08	+0.08	+0.08	+0.08
C(9a)	–0.16	–0.16	–0.16	–0.16	–0.16	+0.27	+0.26	+0.26	+0.25	+0.25
C(9b)	+0.08	+0.10	+0.11	+0.13	+0.14	–0.11	–0.11	–0.10	–0.09	–0.09

Table 32. Energy and geometric characteristics of the possible adducts of (**101**) (R = H) with a proton

Protonation Site	$-E_{rel}$ /kcal mol^{-1}	Bond length/Å
N (1)—H	75.1	1.394
C (3)—H	42.9	1.363
N (4)—H	0.0	1.543
C (5)—H	27.7	1.472
C(6a)—H	27.5	1.412
C (8)—H	37.7	1.361
C(9a)—H	21.9	1.361

Table 33. Total energies (E_{tot}), the relative total energies (E_{rel}), and the Gibbs free energies (ΔG) calculated for the gas phase of systems (103) (R = H), (**104**), (**105**), and (**107**) and the relative Gibbs free energies calculated with inclusion of the solvent effect (ΔG_{solv})

System	$-E_{tot}$/au	$-E_{rel}$/ Kcal.mol^{-1}	$-\Delta G$ Kcal.mol^{-1}	$-\Delta G_{solv}$ Kcal.mol^{-1}
104	886.65267	208.1	110.3	237.9
TS1	886.52220	126.2	86.6	166.8
105	886.58022	162.6	94.6	192.2
TS2	886.5727	157.9	95.6	191.6

107	886.70620	241.7	120.2	268.1
130+H^+	886.49385	108.4	48.3	8.6

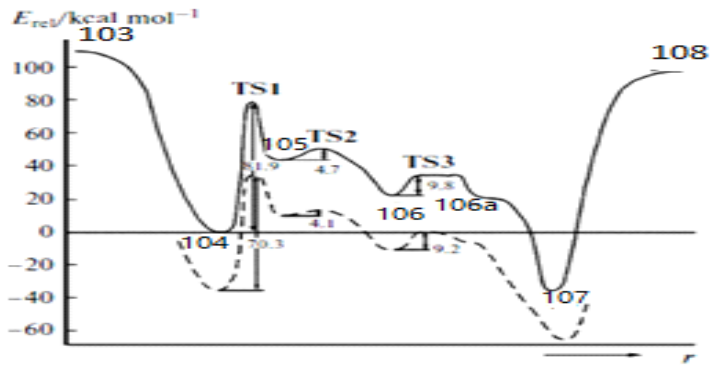

Scheme 19. Potential energy surface along the minimum-energy path for the proton-catalyzed rearrangement (**103**), (**108**) in the gas phase (solid line) and in solution (dashed line); r is the reaction coordinate

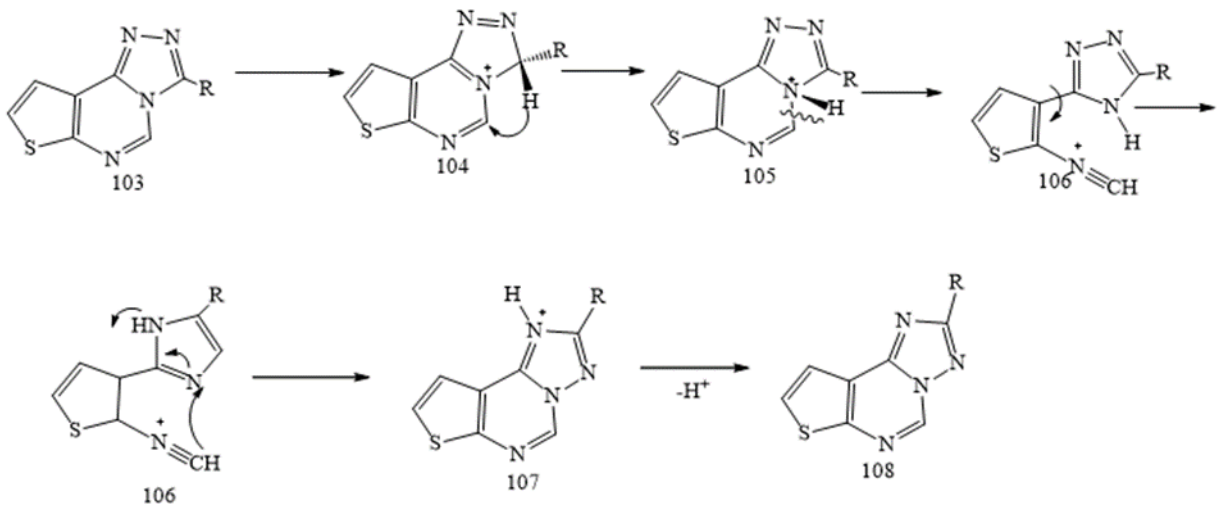

Scheme 20. The proton-catalyzed rearrangement of **(103), (108)**

2.2.12.1. b- Rearrangement in an alkaline medium

The nucleophilic attack on the electron deficient C (5) atom positioned between two electronegative nitrogen atoms, N (4), and N (6), would be predicted to occur already in the first step in an alkaline media, as opposed to an acidic medium. As indicated in **Scheme 20**, this produces anion (**108**). Total energies (E_{tot}), relative total energies (E_{rel}), and Gibbs free energies (G) calculated for the gas phase of systems (**103**) (R = H) and (**108-111**) were displayed in **Scheme 21** and **Table 34**, which displayed total energies (E_{tot}), relative total energies (E_{rel}), and Gibbs free energies (G) calculated for the gas phase of systems (103) (R = H), (108-111), and the relative Gibbs free energies of the solvent effect (ΔG_{solv}). Transition states TS1-TS3 are presented in **Scheme 22**. The total energy of compound **(103)** (R = H) and a hydroxide anion at an infinite distance from each other was taken as the reference point [79].

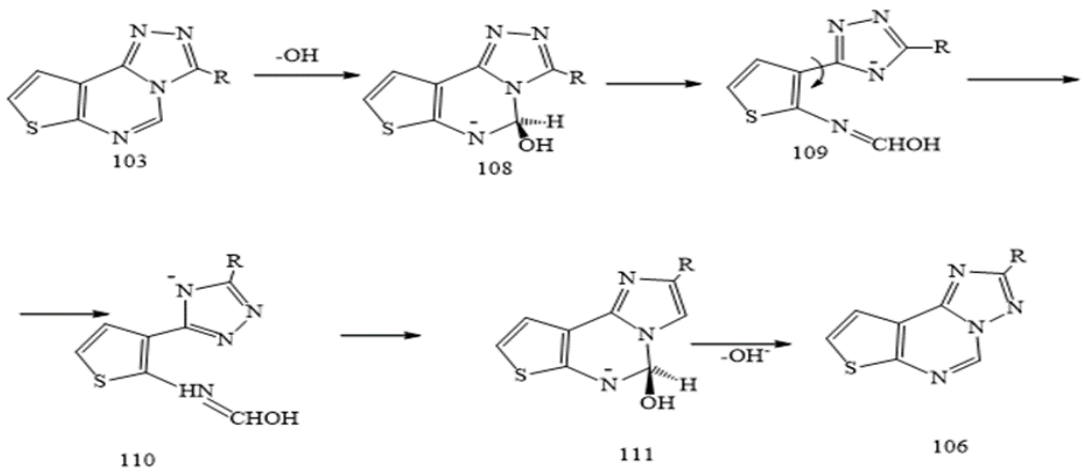

Scheme 21. Anion **108**

Table 34. Total energies (E_{tot}), the relative total energies (E_{rel}), and the Gibbs free energies (ΔG) calculated for the gas phase of systems (**103**) (R = H) and (**108-111**) and the relative Gibbs free energies calculated with inclusion of the solvent effect (ΔG_{solv})

System	$-E_{tot}$ /au	$-E_{rel}$ kcal mol^{-1}	$-\Delta G$	$-\Delta G_{solv}$
108	962.18975	**89.6**	38.3	29.3
TS1	962.17131	78.0	24.0	17.7
109	962.18687	87.8	37.8	29.8
TS2	962.17452	80.0	29.5	25.8
110	962.18855	88.8	38.9	29.9
TS3	962.17029	77.4	26.6	18.2
111	962.19971	95.8	44.0	33.0
108+OH^{-1}	962.1395	58.0	8.7	14.4

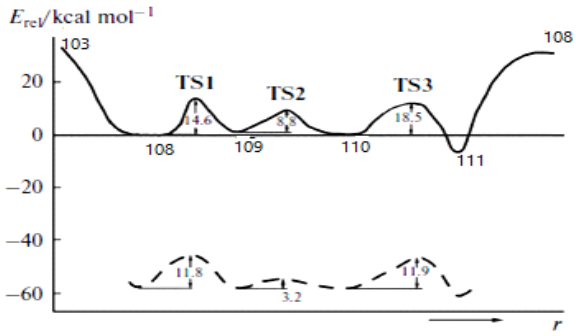

Scheme 22. Potential energy surface along the minimum-energy path for the hydroxide-catalyzed re-arrangement (103, 108) in the gas phase (solid line) and in solution (dashed line); r is the reaction coordinate

3. Conclusion

We extract information about the structures, prosperities, preparations, characterizations, and stability of triazolopyrimidine derivatives from a collection of computer studies. The primary purpose of this research is to see if these chemicals can be used as inhibitors or in drug delivery. Calculations using quantum and molecular mechanics revealed that the inhibition efficiency was linked to quantum chemical parameters. As a result,

triazolopyrimidine derivatives could be considered the lead chemicals for future medical and agrochemical development.

Acknowledgments

Authors would like to thank everyone that contributed to the success of this manuscript and also the Journal of Chemical Review for their tireless efforts.

Orcid:

Hussein S. Mohamed http://orcid.org/0000-0001-8305-0561

References

[1]. G. Fischer, *Adv. Heterocycl. Chem.*, **2007**, *95*, 143-219. [Crossref], [Google Scholar], [Publisher]
[2]. P. Molina, A. Arques, M.V. Vinader, J. Becher, K. Brondum, *J. Org. Chem.*, **1988**, *53*, 4654-4663. [Crossref], [Google Scholar], [Publisher]
[3]. Y. Sato, Y. Shimoji, H. Fujita, H. Nishino, H. Mizuno, S. Kobayashi, S. Kumakura, *J. Med. Chem.*, **1980**, *23*, 927-937. [Crossref], [Google Scholar], [Publisher]
[4]. H. Ohnishi, K. Yamaguchi, S. Shimada, Y. Suzuki, A. Kumagai, *Life Sci.*, **1981**, *28*, 1641-1646. [Crossref], [Google Scholar], [Publisher]
[5]. N. Zhang, S. Ayral-Kaloustian, T. Nguyen, J. Afragola, R. Hernandez, J. Lucas, J. Gibbons, C. Beyer, *J. Med. Chem.*, **2007**, *50*, 319-327. [Crossref], [Google Scholar], [Publisher]
[6]. S.A. Ahmed, A.H. Elghandour, H.S. Elgendy, *Der Pharma Chem.*, **2014**, *6*, 194-219. [Google Scholar], [Publisher]
[7]. H. Mohamed, H. Bhanaswy, S. Ahmed, Evaluation of *N*-Sulfanoamide Pyridines from Chalchon with Anticancer Effect. **2017.** [Crossref], [Publisher]
[8]. M. Song, X. Hao, L. Zhang, M. Song, J. Cheng, Li, D., W. Zhang, J. Wu, *Integr. Environ. Assess. Manag.*, **2021**. [Crossref], [Google Scholar], [Publisher]
[9]. H.M. Ashour, O.G. Shaaban, O.H. Rizk, I.M. El-Ashmawy, *Eur. J. Med. Chem.*, **2013**, *62*, 341-351. [Crossref], [Google Scholar], [Publisher]
[10]. R. Kumar, R.R. Nair, S.S. Dhiman, J. Sharma, O. Prakash, *Eur. J. Med. Chem.*, **2009**, *44*, 2260-2264. [Crossref], [Google Scholar], [Publisher]
[11]. S.A. Ahmed, H.S. Mohamed, W.O. Younis, *ChemInform*, **2015**, *46*. [Google Scholar],
[12]. Q. Chen, X.L. Zhu, L.L. Jiang, Z.M. Liu, G.F. Yang, *Eur. J. Med. Chem.*, **2008**, *43*, 595-603. [Crossref], [Google Scholar], [Publisher]
[13]. X. Deng, S. Kokkonda, F. El Mazouni, J. White, J.N. Burrows, W. Kaminsky, S.A. Charman, D. Matthews, P.K. Rathod, M.A. Phillips, *J. Med. Chem.*, **2014**, *57*, 5381-5394. [Crossref], [Google Scholar], [Publisher]
[14]. T. Novinson, R. Springer, D.E. O'Brien, M.B. Scholten, J.P. Miller, R.K. Robins, *J. Med. Chem.*, **1982**, *25*, 420-426. [Crossref], [Google Scholar], [Publisher]
[15]. S.A. Ahmed, H.S. Elgendy, W.O. Younis, Pyrazolopyrimidines: Synthesis, Chemical Reactions and Biological Activity. *ChemInform*, **2015**, *46.* [Google Scholar], [Publisher]
[16]. D.A. Abdelrheem, A.A. Rahman, K.N. Elsayed, H.R. Abd El-Mageed, H.S. Mohamed, S.A. Ahmed, *J. Mol. Struct.*, **2021**. *1225*, 129245. [Crossref], [Google Scholar], [Publisher]
[17]. E.R. da Silva, N. Boechat, L.C. Pinheiro, M.M. Bastos, C.C. Costa, J.C. Bartholomeu, T.H. da Costa, *Chem. Biol. Drug Des.*, **2015**, *86*, 969-978. [Crossref], [Google Scholar], [Publisher]
[18]. A.B. Caballero, A. Rodríguez-Diéguez, M. Quirós, J.M. Salas, Ó. Huertas, I. Ramírez-Macías, F. Olmo, C. Marín, G. Chaves-Lemaur, R. Gutierrez-Sánchez, M. Sánchez-Moreno, *Eur. J. Med. Chem.*, **2014**, *85*, 526-534. [Crossref], [Google Scholar], [Publisher]
[19]. I.A. Khalymbadzha, T.S. Shestakova, J.O. Subbotina, O.S. Eltsov, A.A. Musikhina, V.L. Rusinov, O.N. Chupakhin, I.L. Karpenko, M.V. Jasko, M.K. Kukhanova, S.L. Deev, *Tetrahedron*, **2014**, *70*, 1298-1305. [Crossref], [Google Scholar], [Publisher]
[20]. I. Personali, **1975**. [Google Scholar], [Publisher]
[21]. L. Wang, Y. Tian, W. Chen, H. Liu, P. Zhan, D. Li, H. Liu, E.D. Clercq, C. Pannecouque, Li, X. Liu, *Eur. J. Med. Chem.*, **2014**, *85*, 293-303. [Crossref], [Google Scholar], [Publisher]
[22]. B. Huang, C. Li, W. Chen, T. Liu, M. Yu, L. Fu, Y. Sun, H. Liu, E.D. Clercq, C. Pannecouque, J. Balzarini, P.Zhan, X. Liu, *Eur. J. Med. Chem.,* **2015**, *92*, 754-765. [Crossref], [Google Scholar],

[Publisher]
[23]. R.A. Singer, J.A. Ragan, P. Bowles, E. Chisowa, B.G. Conway, E.M. Cordi, K.R. Leeman, L.J. Letendre, J.E. Sieser, G.W. Sluggett, C.L. Stanchina, H. Strohmeyer, J. Blunt, S. Taylor, C. Byrne, D. Lynch, S. Mullane, M.M. O'Sullivan, M. Whelan, *Org. Process Res. Dev.*, **2014**, *18*, 26-35. [Crossref], [Google Scholar], [Publisher]
[24]. R.P. Brigance, W. Meng, A. Fura, T. Harrity, A. Wang, R. Zahler, M.S. Kirby, L.G. Hamann, *Bioorg. Med. Chem. Lett.*, **2010**, *20*, 4395-4398. [Crossref], [Google Scholar], [Publisher]
[25]. A.S. Cornec, M.J. James, J. Kovalevich, J.Q. Trojanowski, V.M.Y. Lee, A.B. SmithIII, C. Ballatore, K.R. Brunden, *Bioorg. Med. Chem. Lett.*, **2015**, *25*, 4980-4982. [Crossref], [Google Scholar], [Publisher]
[26]. V.M. Chernyshev, D.A. Pyatakov, A.N. Sokolov, A.V. Astakho, E.S. Gladkov, S.V. Shishkina, O.V. Shishkin, *Tetrahedron*, **2014**, *70*, 684-701. [Crossref], [Google Scholar], [Publisher]
[27]. L. Xiong, Y.Q. Shen, L.N. Jiang, X.L. Zhu, W.C. Yang, W. Huang, G.F. Yang, *ACS Symposium Series*, **2015**, *1204*, 175-194. [Crossref], [Google Scholar], [Publisher]
[28]. M. Rodriguez-Torres, E.M. Yoshida, P. Marcellin, S. Srinivasan, V.S. Purohit, C. Wang, J.L. Hammond, *Ann. Hepatol.*, **2014**, *13*, 364-375. [Google Scholar], [Publisher]
[29]. A.A. Bayazeed, R.B. Alnoman, *Polycycl. Aromat. Compd.*, **2020**, 1-14. [Crossref], [Google Scholar], [Publisher]
[30]. A. El-satar, S. Shireen, N.E. Nasr, K.A. Khailo, H.E. Sayour, *Slov. Vet. Res.*, **2019**, *56*. [Google Scholar], [Publisher]
[31]. S. Li, X. Liu, F. Dong, J. Xu, H. Xu, M. Hu, Y. Zheng, *Food Chem.*, **2016**, *192*, 893-899. [Crossref], [Google Scholar], [Publisher]
[32]. M. Stanić, S. Križak, M. Jovanović, T. Pajić, A. Ćirić, M. Žižić, J. Zakrzewska, T.C. Antić, N. Todorović,M. Živić, *Microbiology*, **2017**, *163*, 364-372. [Crossref], [Google Scholar], [Publisher]
[33]. A.B. Caballero, A.R. Diéguez, M. Quirós, L. Lezama, J.M. Salas, *Inorg. Chim. Acta*, **2011**, *378*, 194-201. [Crossref], [Google Scholar], [Publisher]
[34]. S. Selim, M. Abdel-Mawgoud, T. Al-sharary, M.S. Almuhayawi, M.H. Alruhaili, S.K. Al Jaouni, M. Warrad, H.S. Mohamed, N. Akhtar, H. AbdElgawad, *Agronomy*, **2022**, *12*, 54. [Crossref], [Google Scholar], [Publisher]
[35]. J.G. Małecki, R. Kruszynski, *Polyhedron*, **2010**, *29*, 1023-1028. [Crossref], [Google Scholar], [Publisher]
[36]. F. Yaccoubi, H. Elleuch, H.S. Mohamed, Z.S. Hamza, Y.H. Zaki, *Molbank*, **2022**, *2022*, M1342. [Crossref], [Google Scholar], [Publisher]
[37]. J.A. Dobado, S. Grigoleit, J.M. Molina, *J. Chem. Soc., Perkin Trans.*, **2000**, *2*, 1675-1680. [Crossref], [Google Scholar], [Publisher]
[38]. S.M. Hamed, W.N. Hozzein, S. Selim, H.S. Mohamed, H. AbdElgawad, *J. Hazard. Mater.*, **2021**, *402*, 123787. [Crossref], [Google Scholar], [Publisher]
[39]. H. Moustafa, M.F. Shibl, R. Hilal, L.I. Ali, S.A. Halim, *Int. J. Spectrosc.*, **2011**, *2011*. [Crossref], [Google Scholar], [Publisher]
[40]. N.K. Soliman, A.F. Moustafa, H.R. Abd El-Mageed, O.F. Abdel-Gawad, E.T. Elkady, S.A. Ahmed, H.S. Mohamed, *Sci. Rep.*, **2021**, *11*, 10000. [Crossref], [Google Scholar], [Publisher]
[41]. V.M. Chernyshev, A.G. Vlasova, A.V. Astakhov, S.V. Shishkina, O.V. Shishkin, *J. Org. Chem.*, **2015**, *80*, 375-385. [Crossref], [Google Scholar], [Publisher]
[42]. A. Astakhov, V. Chernyshev, *Chem. Heterocycl. Comp.*, **2012**, *48*, 1417-1419. [Crossref], [Google Scholar], [Publisher]
[43]. A. Astakhov, R.I. Zubatyuk, R.S. Abagyan, V.M. Chernyshev, *Chem. Heterocycl. Comp.*, **2014**, *49*, 1500-1507. [Crossref], [Google Scholar], [Publisher]
[44]. A. Salgado, C. Varela, A.M.G. Collazo, F. García, P. Pevarello, I. Alkorta, J. Elguero, *J. Mol. Struct.*, **2011**, *987*, 13-24 [Crossref], [Google Scholar], [Publisher]
[45]. O. Prakash, V. Bhardwaj, R. Kumar, P. Tyagi, K.R. Aneja, *Eur. J. Med. Chem.*, **2004**, *39*, 1073-1077. [Crossref], [Google Scholar], [Publisher]
[46]. H.C. Van der Plas, *Acc. Chem. Res.*, **1978**, *11*, 462-468. [Crossref], [Google Scholar], [Publisher]
[47]. H.C. van der Plas, *Chem. Heterocycl. Compd.*, **1994**, *30*, 1427-1443. [Crossref], [Google Scholar], [Publisher]
[48]. H.M.E. Hassaneen, T.A. Farghaly, *J. Heterocycl. Chem.*, **2015**, *52*, 1154-1161.

[49]. [Crossref], [Google Scholar], [Publisher]
[50]. G.J. DeBoer, S. Thornburgh, J. Gilbert, R.E. Gast, *Pest Manag. Sci.*, **2011**, *67*, 279-286. [Crossref], [Google Scholar], [Publisher]
[51]. K.S. Shikhaliev, D.V. Krylski, A.Y. Potapov, S.E. Nefedov, O.E. Sidorenko, *Russ. Chem. Bull.*, **2008**, *57*, 1268-1272. [Crossref], [Google Scholar], [Publisher]
[52]. D.D. Diaz, W.G. Lewis, M. Finn, *Synlett*, **2005**, *2005*, 2214-2218. [Crossref], [Google Scholar], [Publisher]
[53]. D.J. Brown, T. Nagamatsu, *Aust. J. Chem.*, **1977**, *30*, 2515-2525. [Crossref], [Google Scholar], [Publisher]
[54]. M. Karabacak, E. Kose, A. Atac, A.M. Asiri, M. Kurt, *J. Mol. Struct.*, **2014**, *1058*, 79-96. [Crossref], [Google Scholar], [Publisher]
[55]. S. Mozafari, A. Shiri, M. Bakavoli, M. Akbarzadeh, K. Saadat, Y. Etemadi, *J. Chem. Res.*, **2016**, *40*, 633-636. [Crossref], [Google Scholar], [Publisher]
[56]. M. Akbarzadeh, et al., *J. Heterocycl. Chem.*, **2016**, *53*, 832-839. [Crossref], [Google Scholar], [Publisher]
[57]. T. Asghari, et al., *Chem. Biol. Drug Des.*, **2015**, *85*, 216-224. [Crossref], [Google Scholar], [Publisher]
[58]. V.M. Chernyshev, V.A. Rakitov, V.A. Taranushich, V.V. Blinov, *Chem. Heterocycl. Compd.*, **2005**, *41*, 1139-1146. [Crossref], [Google Scholar], [Publisher]
[59]. M.A. Girasolo, D. Schillaci, C. Di Salvo, G. Barone, A. Silvestri, G. Ruisi, *J. Organomet. Chem.*, **2006**, *691*, 693-701. [Crossref], [Google Scholar], [Publisher]
[60]. H.C. van der Plas, A.R. Katritzky, Advances in Heterocyclic Chemistry. **1999**, Elsevier. [Google Scholar], [Publisher]
[61]. A. Elyoussfi, H. Elmsellem, A. Dafali, K. Cherrak, N.K. Sebbar, A. Zarrouk, E.M. Essassi, A. Aouniti, B.E. Mahi, B. Hammouti, *Der Pharma Chem.*, **2015**, *7*, 284-291. [Google Scholar], [Publisher]
[62]. C. Wang, C. Tang, X. Fang, Z. Li, Q. Wang, *Synlett*, **2015**, *26*, 931-936 [Crossref], [Google Scholar], [Publisher]
[63]. A. Bououidina, F. El-Hajjaji, M. Drissi, M. Taleb, B. Hammouti, I.M. Chung, S. Jodeh, H. Lgaz, *Metall. Mater. Trans. A*, **2018**, *49*, 5180-5191. [Crossref], [Google Scholar], [Publisher]
[64]. K. Khaled, et al., *J. Mater. Environ. Sci.*, **2011**, *2*, 166-173. [Google Scholar]
[65]. A. Hazrathoseyni, S.M. Seyedi, A. Shiri, H. Eshghi, *J. Chem. Res.*, **2015**, *39*, 148-153. [Crossref], [Google Scholar], [Publisher]
[66]. S. Bagherifam, **2013**. [Google Scholar], [Publisher]
[67]. A.N. Abulhail, W.A. Radhi, M.J. Meften, *Basrah j. sci.*, **2018**, *36*, 1-30. [Google Scholar], [Publisher]
[68]. X. Wu, X. Wu, Q. Sun, C. Zhang, S. Yang, L. Li, Z., Jia, *Theranostics*, **2017**, *7*, 826. [Crossref], [Google Scholar], [Publisher]
[69]. V.M. Chernyshev, D.A. Khoroshkin, A.N. Sokolov, V.A. Taranushich, E.S. Gladkov, S.V. Shishkina, O.V. Shishkin, S.M. Desenko, *J. Heterocycl. Chem.*, **2008**, *45*, 1419-1427. [Crossref], [Google Scholar], [Publisher]
[70]. A.N. Sokolov, M.S. Mischenko, E.S. Gladkov, V.M. Chernyshev, *Chem. Heterocycl. Comp.*, **2011**, *47*, 249-251. [Crossref], [Google Scholar], [Publisher]
[71]. V.A. Chebanov, S.M. Desenko, T.W. Gurley, Azaheterocycles based on a, ß-unsaturated carbonyls, **2008.** [Google Scholar], [Publisher]
[72]. M.O. Shyshkina, S.V. Shishkina, K.S. Ostras, N.Y. Gorobets, V.A. Chebanov, S.M. Desenko, *Acta Cryst. E: Crystallogr. Commun.*, **2021**. *77*, 1323-1326. [Crossref], [Google Scholar], [Publisher]
[73]. R.V.A. Orru, E. Ruijter, **2010**, *2*, Springer Science & Business Media. [Google Scholar], [Publisher]
[74]. B. Machura, A. Świtlicka, M. Wolff, J. Kusz, R. Kruszynski, *Polyhedron*, **2009**, *28*, 1348-1354. [Crossref], [Google Scholar], [Publisher]
[75]. T. Nagamatsu, Chemical Studies of Some Triazolopyrimidines. **1979**, The Australian National University. (Australia) [Crossref], [Google Scholar], [Publisher]
[76]. M. Bakavoli, S.M. Seyedi, A. Shiri, S. Saberi, M. Gholami, H. Sadeghian, *J. Chem. Res.*, **2013**, *37*, 48-50. [Crossref], [Google Scholar], [Publisher]
[77]. S. Karki, T. Friščić, L. Fabian, P.R. Laity, G.M. Day, W. Jones, *Adv. Mater.*, **2009**, *21*, 3905-3909. [Crossref], [Google Scholar], [Publisher]
[78]. H.S.H. Mohamed, S.A. Ahmed, *J. Chem. Rev.*, **2019**, *1*, 183-232. [Crossref], [Google Scholar], [Publisher]
[79]. I. Lukovits, E. Kalman, F. Zucchi, *Corrosion*, **2001**, *57*, 3-8. [Crossref], [Google Scholar], [Publisher]
[80]. N.M. O'boyle, A.L. Tenderholt, K.M.

Langner, *J. Comput. Chem.*, **2008**, *29*, 839-845. [Crossref], [Google Scholar], [Publisher]
[81]. S.A. Ahmed, A.A. Rahman, K.N. Elsayed, H.R. Abd El-Mageed, H.S. Mohamed, S.A. Ahmed, *J. Biomol. Struct. Dyn.*, **2021**, *39*, 3855-3873. [Crossref], [Google Scholar], [Publisher]

Hussein S. H. Mohamed: He was born Beni-Suef (Egypt) in 1980, obtained his Ph.D. degree in Organic chemistry in 2015 under the supervisor of Prof. Dr. Ahmed Elghandour and Prof. Dr. Sayed A. Ahmed. Later on, he is currently working as Head of Basic sciences department , HIGHER TECHNOLOGICAL INSITUTE – BENI SUEF , Senior Researcher in Natural Products of Research Institute of Medicinal and Aromatic Plants (RIMAP), Beni-Suef University. He has been actively involved synthesis of heterocyclic compounds and its applications in biological activities, recently he interested in removal of dyes and heavy metals from wastewater by different synthesized compounds.

Zeinab shaaban Hamza: I am hold a Bachelor of Science degree in geology and chemistry department and I am a master's student in the field of chemistry of medicinal and aromatic plants.

Amany Mohamed Nagdy: I am hold a Bachelor of Science degree in special chemistry department and I am master's student in the field of organic chemistry.

Hamada Rezk Abd El-Mageed: I am hold a Bachelor of Science degree in chemistry department and master degree in the field of physical chemistry.